

Modelling the impacts of future enhanced winter warming events on subarctic ecosystems using LPJ-GUESS

Didac Pascual¹, Margareta Johansson¹, Jing Tang¹, and Alexandra Pongracz¹

¹Lund University

December 7, 2022

Abstract

Winter warming events (WWEs) are short-lasting events of unusually warm weather, occasionally combined with rainfall, which can cause severe ecosystem impacts by altering ground temperatures and water fluxes. These impacts are generally overlooked in large-scale ecosystem models. The frequency and intensity of WWEs will likely increase further in the future. We used an ecosystem model, LPJ-GUESS, to investigate the responses of four subarctic ecosystems to different levels of predicted WWEs, and identify model gaps hindering accurate estimates of these responses. In response to WWEs, the model simulated substantial ground cooling (up to 2 °C in winter) in contrast to the observed warming, leading to changes in biogeochemical fluxes often comparable in magnitude to those from altered winter climatologies. The mismatch between the modelled and the observed ground temperature changes may be due to the 1) lacking surface energy balance, 2) daily timestep, and 3) simplistic water retention scheme in LPJ-GUESS.

D. Pascual^{1*}, M. Johansson¹, A. Pongracz¹, & J. Tang^{1,2}

¹Department of Physical Geography and Ecosystem Science, Lund University, Lund Sweden

²Section of Terrestrial Ecology, Department of Biology, University of Copenhagen. Copenhagen, Denmark

* Corresponding author. E-mail: Didac.pascual@nateko.lu.se - Affiliation address: Sölvegatan 12, 223 62 Lund, Sweden - Telephone dir 0046 720324595

Key Points:

- Winter warming events (WWEs) have increased in the Arctic and are expected to increase further, but their impacts are not thoroughly evaluated in large-scale ecosystem models.
- We applied different scenarios of enhanced WWEs in a widely used ecosystem model, LPJ-GUESS, and found that their impacts on ecosystem processes could be substantial and of magnitudes comparable to those of altered winter climatologies.
- The direction of the modeled WWE impacts on ground temperatures differed from what the observation-based literature suggests, and we identified essential processes lacking in LPJ-GUESS that may cause this mismatch.

Abstract

Winter warming events (WWEs) are short-lasting events of unusually warm weather, occasionally combined with rainfall, which can cause severe ecosystem impacts by altering ground temperatures and water fluxes. These impacts are generally overlooked in large-scale ecosystem models. The frequency and intensity of WWEs will likely increase further in the future. We used an ecosystem model, LPJ-GUESS, to investigate the responses of four subarctic ecosystems to different levels of predicted WWEs, and identify model gaps hindering accurate estimates of these responses. In response to WWEs, the model simulated substantial

ground cooling (up to 2 °C in winter) in contrast to the observed warming, leading to changes in biogeochemical fluxes often comparable in magnitude to those from altered winter climatologies. The mismatch between the modelled and the observed ground temperature changes may be due to the 1) lacking surface energy balance, 2) daily timestep, and 3) simplistic water retention scheme in LPJ-GUESS.

Plain Language Summary

In the Arctic, winter warming events (WWEs) are episodes of exceptionally warm weather that last from hours to a few days and often occur in combination with rainfall. The combined effect of multiple processes triggered by WWEs (involving, for example, changes in snow depth and snow properties, and heat exchanges between air, rain and meltwater, and soils) results in profound changes in ground temperatures and water fluxes, which many ecosystem processes depend on (vegetation dynamics, organic matter decomposition by microbes, etc). However, large-scale ecosystem models, which are used to study how arctic ecosystems will change in the future, often overlook the effects of WWEs because they oversimplify some complex physical processes and operate at longer temporal scales than WWEs. WWEs will likely become more frequent and intense in the future as the climate continues to warm. This study used a widely used ecosystem model, LPJ-GUESS, to investigate how the ecosystems will respond to more frequent and intense WWEs. The ecosystem responses that we observed were notable but in the opposite direction as observed in field measurements. We identified the processes that are lacking in the model and are causing this mismatch which, if implemented in the model, would significantly improve the predictions of future ecosystem changes in response to climate change.

1 Introduction

The Arctic is warming three times faster than the global average, with the strongest warming occurring in autumn and winter (AMAP 2021). The occurrence and impacts of winter warming events (WWEs), i.e. short-lasting extraordinarily warm spells, often accompanied by rainfall (rain on snow; ROS), are increasing rapidly and expanding geographically (e.g. Bartsch et al., 2010; Vikhamar-Schuler et al., 2016; Pan et al., 2018). Climate models predict a further increase in the coming decades. Despite their short duration, these extreme events could cause societal and environmental impacts that can override the impacts of long-term climatic trends (e.g., Phoenix & Bjerke, 2016).

In the winter, the impacts of WWEs are currently considered a research priority for better understanding future ecosystem dynamics in the subarctic (Pascual et al., 2020). WWEs can affect ground temperatures (GT) in multiple ways, mostly through: (1) direct heat transfer from the air, (2) latent heat release from refreezing melt and rainwater, and (3) changing the snowpack properties, such as depth and density, which influence the energy exchanges between the atmosphere, snow, and soil. These altered winter processes can further influence ground albedo and groundwater content (GWC), which has impacts lasting to the growing seasons (Pascual & Johansson, 2022). These WWE-associated environmental changes can further alter microbial activity, greenhouse gas (GHG) emissions (e.g., Natali et al., 2019), and permafrost and vegetation dynamics (Bruhwiler et al., 2021), ultimately altering the arctic carbon budget.

These interlinked processes and feedbacks related to WWEs are difficult to disentangle in observational data and thus challenging to implement in models. Moreover, large-scale ecosystem models which run with monthly climate data do not explicitly account for the impacts of such stochastic climate extremes (e.g. Tang et al., 2015).

In this study, we investigate the potential effects of predicted WWE scenarios on winter and growing-season physical and biogeochemical variables using the latest version of a widely used dynamic ecosystem model, LPJ-GUESS. We aim to evaluate the model's performance and identify model gaps in representing ecosystem responses to future WWEs.

2 Materials and Methods

2.1 Study sites

The Torneträsk area, in northern Sweden, is a topographically heterogeneous area that aligns along a strong west-east oceanic-continental climatic gradient, with precipitation and winter temperature decreasing eastwards due to the increasing continentality and the rain shadow effect caused by the Scandes Mountains. The area has experienced rapid climate warming (Callaghan et al., 2010) and a substantial increase in the frequency and intensity of WWEs (Pascual & Johansson, 2022).

Vegetation in the area varies following its climatic and altitudinal gradients. Birch forests occur below c. 600 and 800 m.a.s.l (Van Bogaert, 2010). Tundra species dominate above the tree-line, while in the lowlands, birch forests alternate with peat plateaus underlain by permafrost, and non-permafrost fens.

In this modelling study, we selected four sites representing these dominant ecosystem types in the Torneträsk area, including (1) a birch forest (~370 m.a.s.l) located <10 km east of the Abisko Station (ANS) (Heliasz et al., 2012); (2) a tundra site (~410 m.a.s.l), located <1 km to the southeast of the ANS (Michelsen et al., 2012 and references therein); (3) a peat plateau (~380 m.a.s.l) known as Storflaket, located c. 6 km east of the ANS (Johansson et al., 2013), and (4) a fen (~515 m.a.s.l) located c. 25 km west of the ANS, near the Katterjokk Station (SMHI). The dominant vegetation species at these sites are found in Appendix A.

2.2 Model description and simulation setup

2.2.1 Model description

The Lund-Potsdam-Jena General Ecosystem Simulator (LPJ-GUESS) is a process-based dynamic ecosystem model widely used on regional and global scale studies (Smith et al., 2001; 2014). The model simulates vegetation dynamics (including vegetation establishment, mortality and competition, etc.), water, carbon and nitrogen cycles, and soil biogeochemistry. This study used the latest version of LPJ-GUESS (version 4.1, Smith et al., 2014), with the recently-developed dynamic, intermediate complexity snow scheme enabling the simulation of climate-snow-soil interaction. The model can simulate up to five snow layers, their physical and thermal properties, and their development throughout the cold season. Based on the individual snow layer properties (e.g., temperature, density, thermal conductivity), freeze-thaw processes in snow layers, and heat transport through the snowpack between the atmosphere and soil can be simulated, and ROS events can be accounted for (Pongracz et al., 2021). LPJ-GUESS includes detailed representations of permafrost and wetland processes, including peatland hydrology, peatland-specific PFTs, and CH₄ emissions (see Wania et al., 2009a, 2009b, 2010).

2.2.2 Model setup

Daily climate data provided by the ANS (ANS 2020) and Katterjokk Station (SMHI), including air temperature, air temperature daily range, and precipitation, together with shortwave radiation (1913-1984, Sheffield et al., 2006; 1984-2018, ANS) and annual CO₂ concentrations obtained from the Global Monitoring Laboratory (<https://gml.noaa.gov/ccgg/trends/>), were used to drive the model from 1913 to 2018. Soil property data was extracted from the WISE5min, V1.2 Soil Property Database (Batjes 2012). More details about the setup and input data are found in Appendix B.

Representative plant functional types (PFTs) were selected for each site (Table A1). We enabled high-latitude and wetland-specific plant functional types (PFTs) in the simulations to better capture site-specific vegetation conditions (see Wania et al., 2009 for more details). The PFT parameters at each site followed previous studies (e.g., Tang et al., 2015; Gustafson et al., 2021) (Table A2).

2.2.3 Model calibration and evaluation

Sobol sensitivity analyses (SA) were conducted to explore the influence of different parameters and parameter interactions on the estimated seasonal snow density, snow depth, snow temperature, and GT at the study sites (except for the tundra site due to lack of observational data for calibration and evaluation) (Appendix D). A sampling of eight relevant parameters, using ranges based on literature values, and a certain percentage of changes from the original values (Table D1), was conducted. Among the most influential parameters, we selected the parameter values that minimized the absolute differences between the measured and the modeled

seasonal snow depth and GT at each site (2006-2012 at the peat plateau, 2001-2010 elsewhere) (Figures D4-8). The model was subsequently evaluated with independent observational data (2011-2018) when possible (Appendix E).

2.2.4 Model simulations with future WWEs

We generated manipulation experiments with different levels of WWE frequencies and intensities imposed on the observation-based climate inputs (HISTORICAL dataset) to assess the responses of different ecosystem processes to these extreme events. The applied frequencies and intensities were based on different climate scenarios in the Coupled Model Intercomparison Project Phase 6 (CMIP6) (Eyring et al., 2016). We selected six climate scenarios from two general circulation models (GCMs) with different climate sensitivities, i.e., CanESM5 and GFDL-ESM4, and three shared socioeconomic pathways representing three levels of varying GHG projections, i.e., SSP119, SSP270, and SSP585. For each scenario (n=6), daily meteorological data (1950-2100) for the gridcell near the Torneträsk area was extracted, and then bias-corrected at a daily scale. Detailed descriptions of the CMIP6 scenarios and the bias-correction method are found in Appendix C.

The bias-corrected GCM's outputs were used to create the manipulation experiments (Table 1). In addition to the HISTORICAL runs (S0), we designed three additional experiments in which the future monthly anomalies in the frequency and intensity of melt days (S1), ROS (S2), and both (S3) in the GCM's outputs (Table C2) were added to the HISTORICAL climate inputs, maintaining the long-term climate means as unchanged as possible. These anomalies were calculated based on four indices modified from Vikhamar et al. (2016) (Table C1).

The effects of altered WWEs and those from the altered long-term climate trends were compared by using an additional experiment (S4) in which the future winter monthly anomalies (Table C3) were directly added to the historical daily air temperature and precipitation.

Table 1 . *Description of the HISTORICAL and MANIPULATION runs.*

Simulation names	Description
S0	HISTORICAL scenario
S1	Altered melt days frequency (WWE index 1 = n days with $T > 0^{\circ}\text{C}$) and intensity (WWE index 2 =
S2	Altered ROS frequency (WWE index 3 = n days with $T > 0^{\circ}\text{C}$, and $P > 1$ mm) and intensity (WW
S3	Altered frequency and intensity of both melt days and ROS (indices 1, 2, 3 & 4)
S4	Altered winter climatologies

Note. T and P refer to air temperature and precipitation. The monthly anomalies were calculated for November to March based on periods of 2071-2100 and 1985-2014.

3 Results and discussion

3.1 Sensitivity analyses and model calibration

The Sobol indices showed that the dens_min (minimum snow density) and compaction_rate (the rate at which snow is compacted over time), and their interactions, mainly influence the modelled seasonal snow depth, snow density, snow temperature, and GT (Figure D1-3).

The parameter values yielding the lowest measured-modelled differences in seasonal snow depth and GT are 50, 60, and 90 for dens_min, and 0.5, 0.8, and 0.9, for compaction_rate, at the birch forest, peat plateau, and fen sites, respectively (Figure D4-8).

For the tundra site, we applied parameter values of 90 and 0.8 for minimum snow density and compaction rate, as these showed the best agreement with the available growing-season observational data.

3.2 Evaluation of physical and biogeochemical variables in the historical period

3.2.1 Evaluation of physical variables

The seasonal patterns of snow cover were captured in the model at all sites. However, snowpack depth was considerably underestimated at the birch forest and the low-elevated fen site, but overestimated in low vegetation settings such as the peat plateau (Figure E1), likely due to the model lacking lateral transport and trapping/deposition of wind-blown snow. This mismatch affected the snow insulating capacity and caused substantial cold and warm biases in winter GT in the birch forest and peat plateau, respectively, but not in the fen (Figure E2) where the modelled snowpack depth exceeds the depth of the maximum insulating effect (40 cm; Zhang, 2005). The growing season GT was well captured at the birch forest and fen sites, but was underestimated in the peat plateau (Figure E2a,c,d).

The model was able to simulate short-term fluctuations in snow depth and GT during WWEs at all sites, but not their magnitudes (Figure E3). At the birch forest and peat plateau, larger than measured fluctuations in GT were modeled during WWEs and these differences were much smaller in the late winters. The modelled differences were largely linked to the simulated insulating capacity of snowpacks. Noticeably, stronger modeled reductions in snow depth occurred during early- and mid-winter WWEs, when the energy needed to warm-up and subsequently melt the thin and fresh (less dense) snowpacks is smaller. The modeled and measured GTs at the fen site remained around 0 °C throughout the winter due to the strong insulation of the thick snowpack, but the model captured the observed snowpack responses to WWEs.

3.2.2 Evaluation of biogeochemical variables

The modeled maximum LAI of 1.6 and 1.5 fell within the observed ranges at the birch forest (Heliasz, 2012) and tundra sites (Simin et al., 2021). Following the biases in GT, winter CO₂ heterotrophic respiration (R_h) was underestimated at the birch forest and overestimated at the peat plateau (Figure E4). We speculate an overestimation of winter R_h at the tundra –it presents similar winter R_h values than the fen and peat plateau, and 6-fold larger than the birch forest– due to the overestimated soil C pool at this site. The model underestimated the growing-season ecosystem respiration (R_{eco}) and gross primary production (GPP) in the tundra (Figure E5c,d). At the birch forest, the model predicted a strong annual C sink in 2007-2010, but measurements indicated a fairly neutral C balance (Figure E4a,b). At the peat plateau and fen sites, the model captured the annual fluctuations and magnitudes of CO₂ fluxes (Figure E4c-f). Across four sites the model was unable to capture the observed strong C source in September.

The differences in CH₄ fluxes between the peat plateau and fen sites were well captured by the model. However, the model underestimated by 55% the winter CH₄ fluxes at the peat plateau, likely due to the colder bias in modeled GT (Figure E6a,b).

3.3 Effects of enhanced WWEs

3.3.1 Impacts on physical variables

The WWE experiments (S1-S3) caused an overall reduction in winter GT (up to 2 °C) in all ecosystem types, except for the runs driven by WWEs from CanESM5 SSP585 at the tundra and the peat plateau (Figure 1a-d). The modeled snow depth also decreased substantially under all WWE experiments. This might suggest that the major driver of the modelled WWE effects on winter GT is snow insulation, which decreases as a combination of the snowpack depth reduction, and the increased thermal diffusivity (caused by higher thermal conductivity and lower heat capacity after freeze-thaw processes), facilitating the heat exchange between atmosphere and soil (Figure 3). However, a “tipping point” may be crossed above a certain WWE magnitude, when the strong cooling effects of the reduced snow insulating capacity are counteracted by the stronger warming effects of longer and more extreme WWEs. This point is reached faster under shallow snowpacks where snow insulation is weak and its further reduction has a smaller effect on GT compared to the overall warmer conditions.

In contrast to WWEs, altered future winter climatologies (S4) increased the modeled winter GT at all sites, from less than 1 °C to as much as 4 °C at the birch forest, tundra, and peat plateau in the warmest scenario, i.e., CanESM5 SSP585, despite snowpack reductions of >80%. The modeled GT warming effect diminishes

under thick snowpacks, due to the snow insulation-related process described above: at the fen site (thickest snowpack) we can only see a GT warming under CanESM5 SSP585.

Our results agree with the modelling results by Beer et al., (2018), who suggested that WWEs may cause GT cooling mainly by reducing the snowpack depth. However, there is increasing observational evidence that intense ROS events cause substantial and long-lasting GT warming in winter (e.g., Hansen et al., 2014) through the latent heat released from refreezing of infiltrated water at the bottom of thick snowpacks (Westermann et al., 2011; Pascual et al., 2022). This long-lasting GT warming cannot be captured in LPJ-GUESS due to the lack of essential processes describing the energy and water exchanges between the atmosphere, snowpack, and soil (Figure 3).

In non-winter, the impacts of the manipulation experiments on GT followed those seen for winter GT, although smaller in magnitude (Figure 1e-h). The WWE impacts on non-winter GWC (0-50 cm depth) were marginal except for the fen site (decrease of up to $0.3 \text{ m}^{-3}\text{m}^{-3}$) (Figure F1). GWC affects the thermal properties of soils, and its reduction likely contributed to the larger non-winter GT cooling modeled at the fen. The reduced albedo following an earlier snow cover disappearance can contribute to faster GT warming in spring, but this process is not represented in the current version of LPJ-GUESS.

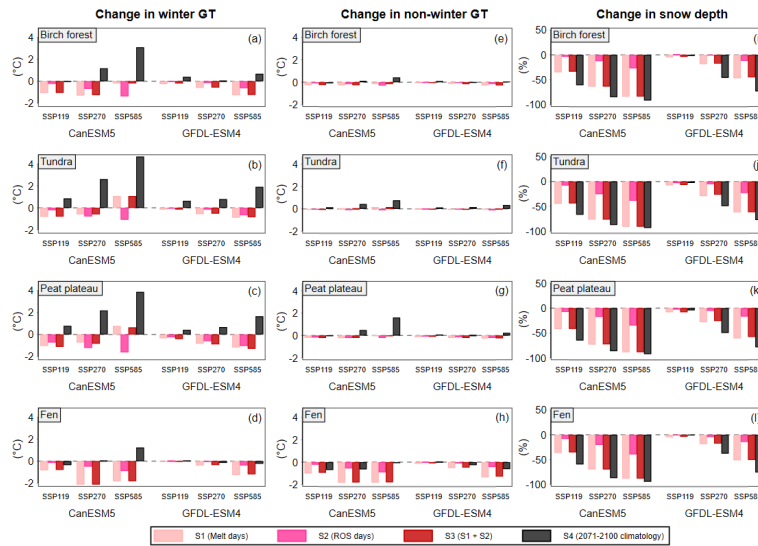


Figure 1 . Differences between the MANIPULATION runs (S1-S4) and the HISTORICAL runs (S0) for winter GT ($^{\circ}\text{C}$; left column), non-winter GT ($^{\circ}\text{C}$; middle column), and winter snow depth (%; right column), at each site.

3.3.2 Impacts on biogeochemical variables

Our results further showed large WWE-induced impacts on all biogeochemical variables, with magnitudes often comparable to impacts deriving from altered winter climatologies (Figures 2 and G3). GT and water availability are key drivers of the ecosystem C cycle, as they influence the start of the growing season, nutrient availability, vegetation dynamics, and soil R_h .

The modelled impacts of the manipulation experiments on biogeochemical variables generally followed the same direction as those observed for GT and GWC. We noted substantial reductions in GPP (Figure 2i-l) under the WWE experiments S1 and S3 of up to 25% at the fen, 20% at the peat plateau, and 10% at the birch site, and smaller reductions under ROS events alone (S2). The tundra site showed weaker reductions in GPP than the other sites, ranging from a few percent to up to 5% in the milder WWE experiments (driven

by SSP119), and increases of up to 10% under CanESM5 SSP585. In contrast, for S4, the model simulated weak changes in GPP in the mildest CMIP6 scenarios, but sizable increases in GPP in the CanESM5 SSP585: up to 75% in the peat plateau, c. 50% in the birch forest, c. 25% in the tundra, and c. 10% in the fen site. The impacts on R_a mirrored those described for GPP (Figure 2e-h). Noticeably, the relationship between GT, and both GPP and R_a , is not linear because the processes involved in plant dynamics are multiple and complex. For example, observational and manipulation studies have reported considerable vegetation damage, delays in bud phenology, and reductions in vegetation greenness due to phenological and frost stress following WWEs (Bokhorst et al., 2009, 2010). These impacts on vegetation are not explicitly represented in the model, as it does not yet take into account these winter/spring stress-related processes.

Increases in GT can stimulate microbial activity and accelerate litter and soil decomposition rates, resulting in increased R_h (Natali et al., 2019). Accordingly, winter R_h increased or decreased by <5% at the fen, and up to 25% at the tundra and peat plateau, following the GT responses (Figure G1). Contrastingly, in response to the CanESM5 SSP585 scenario at the birch forest site, despite the overall lower winter GT, winter R_h increased by up to >200%. This may be explained because the modeled winter R_h in the birch forest is very low (6 g C m⁻², compared to >30 g C m⁻² at the other sites), and even small increases in R_h during WWEs can result in substantial relative increases in winter emissions. A recent synthesis of in situ observations across the Arctic indicates that winter R_h accounts for a substantial portion of the arctic's annual C budget (Natali et al., 2019). Winter R_h alone currently offsets ~40% of the measured annual vegetation C uptake at our sites. Applying the winter R_h response curve to GT by Natali et al., (2019) ($Q_{10} = 2.9$), WWE-induced impacts on winter GT of the magnitudes reported here could change total winter R_h by up to 25%. Hence, realistically simulating the effects of WWEs on GT is important for improving estimates of GHG emissions in high latitudes.

The modelled CH₄ emissions at the peat plateau and fen sites decreased under all WWE experiments due to WWE-induced decreases in GT and GWC (Figure G2). At the fen site, emissions halved mostly due to lower water tables in the non-winter season.

Overall, the year-round ecosystem C exchange (i.e. NEE) of the birch forest, tundra, and peat plateau sites decreased (i.e., became a smaller C sink) considerably under most WWE experiments (Figure G3), generally between 20% and 50%, and up to 90% occasionally in the tundra site, due to larger reductions in vegetation C assimilation compared to the C losses from R_h . Contrastingly, NEE at the fen site increased weakly (i.e., became a stronger C sink), mostly due to large reductions in R_h . Noticeably, the changes in NEE caused by WWEs (S1-S3) are substantial and of similar magnitude to those caused by shifts in future winter climatologies (S4). This further indicates that WWEs, despite their short duration, may have the potential to induce changes in high-latitude ecosystem C cycling of magnitudes comparable to those induced by long-term climatic trends.

Given the observed discrepancies in modeled vs measured GT responses to WWEs (section 3.2.1), the modeled impacts on ecosystems C fluxes reported here should not be interpreted as a direction prediction of future impacts of WWEs, but rather as a sensitivity test of the current model's responses to altered levels of WWEs.

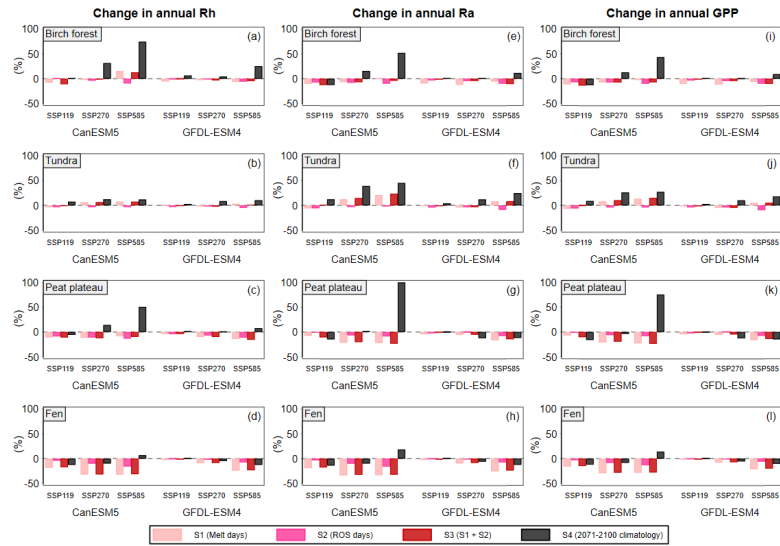


Figure 2. Differences between the MANIPULATION (S1-S4) and the HISTORICAL runs (S0), for annual Rh (%; left column), annual Ra (%; middle column), and annual GPP (%; right column), at each site.

3.4.3 Model limitations and potential developments

LPJ-GUESS has difficulties in capturing the physical changes in snow depth induced by WWEs. We identified the lack of surface energy balance in LPJ-GUESS as one of the main limitations to simulating WWE impacts on GT. Heat transfer between air-snow-soil layers is simulated using the Crank-Nicolson finite difference scheme (Crank and Nicolson, 1996). This indirect method of defining heat transfer may significantly affect the computed snow layer and ground temperatures, and the rate and magnitude of snowmelt events. Additionally, the model’s daily timestep may be too coarse to capture the sub-daily freeze-thaw cycles and hydrological processes within the snowpack.

In the model, heat transfer is affected by the changes in snow layer temperature and thermal properties, and the latent heat release upon freezing is not captured (Figure 3). The SA showed that the current model setup is not sensitive to changes in liquid water holding capacity in snow layers (Figure D1-3), potentially due to the simplistic water retention scheme applied. Rainfall infiltration follows a bucket model approach, limited by each snow layer’s maximum water-holding capacity. Precipitation from ROS events and melt water is quickly forwarded to the soil as runoff at the simulated time step (i.e., daily) when the maximum liquid holding capacity of a layer is reached. If the ground is frozen, the excess liquid water will not stay in the bottom snow layer, but drain out as surface runoff. This feature also prevents the formation of ice layers of high thermal conductivity within the snow layers, as many observational studies suggest (e.g., Langlois et al., 2017), which could influence the simulated GT. Observations suggest major ROS events may have durable impacts on GT (e.g. Westermann et al., 2011), but the current model setup cannot capture such persistent effects due to the simple water retention scheme and the lacking processes related to energy balance.

The LPJ-GUESS version used in this study has an intermediate complexity snow scheme, similar to many ecosystem models. These modules are developed and tuned to represent average conditions rather than capturing extreme and smaller-scale phenomena such as WWEs. There is a need for either further snow scheme development in LPJ-GUESS or evaluating a more complex, designated snow model to address the listed shortcomings and capture internal snow dynamics on a finer spatio-temporal scale. A recent extension of the model with detailed land surface processes and surface energy balance LPJ-GUESS LSMv1.0 (Belda et al., 2022) could be used in future studies to assess whether the model-measurements mismatch is reduced when using the LPJ-GUESS with detailed energy balance and sub-daily processes. This land surface model

version of LPJ-GUESS needs to be thoroughly evaluated and tested in high latitude environments. Regional modelling studies are required to further understand how WWEs might affect the pan-Arctic carbon budget.

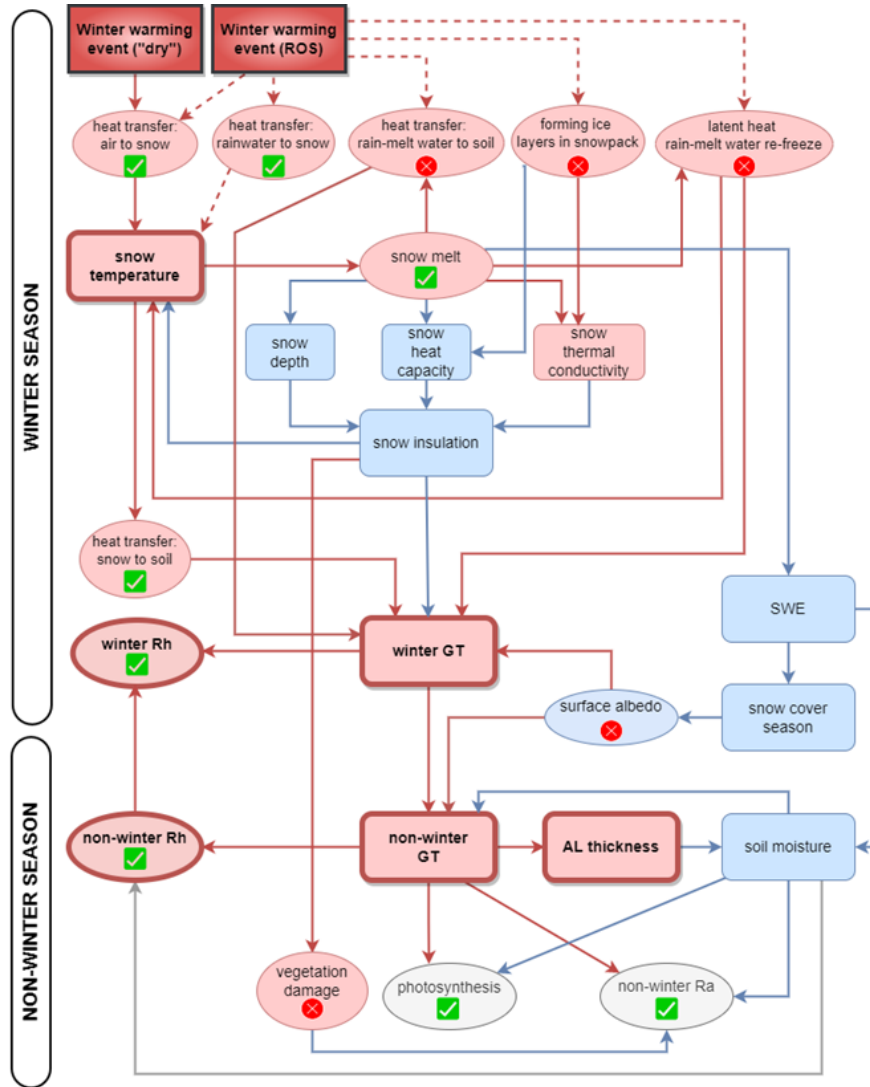


Figure 3. Theoretical model of the WWE impacts. Box colors indicate the overall direction of changes (red=increase, blue=decrease) in the variables based on the literature. Thick outlines and bold text indicate a disagreement between the literature and our simulations. Arrow colors show the direction of the change exerted by each process. Dashed lines refer to ROS-related processes. Grey boxes and lines refer to uncertain processes and responses. Green ticks and red crosses indicate WWE-related processes that are, or are not, implicitly implemented in the current model version.

5 Conclusions

We applied future-simulated WWE experiments in LPJ-GUESS to investigate the potential effects of these events on four dominant ecosystems in subarctic Sweden. The modeled impacts of WWEs on the ecosystem variables were substantial and of magnitudes often comparable to those of altered winter climatologies. These events induced reductions in GT which altered numerous biogeochemical processes and resulted in substantial changes in ecosystem CO₂ uptake. This highlights the need to realistically represent the effects of WWEs in

ecosystem models -which are still largely overlooked especially in regional and large scale studies- to improve estimates of the current and future high-latitude C budget. The direction of the modeled impacts on GT differed from the majority of the observation-based literature. We identified the current model limitations contributing to this mismatch, including 1) the lack of surface energy balance, 2) the model's daily timestep, 3) and the simplistic water retention scheme applied in the LPJ-GUESS snow scheme.

Acknowledgments

Open access funding provided by Lund University. We are grateful to the Department of Physical Geography and Ecosystem Science, Lund University for the grant received to promote research integration and advancement of early-career researchers at the department 2018. We are also grateful to Anders Michelsen for valuable input. This study has been made possible by data provided by the Abisko Scientific Research Station and the Swedish Meteorological and Hydrological Institute (SMHI). J.T. is financially supported by Swedish FORMAS mobility grant (2016-01580) and acknowledges support from Lund University strategic research area Modelling the Regional and Global Earth System, MERGE. A.P acknowledges financial support from the Swedish Research Council (WinterGap, registration no. 2017-05268) and the Research Council of Norway (WINTERPROOF, project no. 274711).

Open Research

The code version used for this study is stored in a central code repository and will be made accessible upon request.

We provided the necessary descriptions for transparency and traceability of the analysis using our community standards.

Observational data used in this study can be retrieved from the following in-text data citation references: ANS (2020) [dataset, accessible upon request], SMHI (2020) [dataset accessible via <https://www.smhi.se/data/utforskaren-oppna-data/?p=1&q=>], Sheffield et al., (2006) [dataset available at <http://hydrology.princeton.edu/>], Global Monitoring Laboratory [dataset available at <https://gml.noaa.gov/ccg/trends/>], Batjes et al., (2012) [dataset available at www.isric.org], Eyring et al., (2016) [dataset accessible at <https://esgf-data.dkrz.de/search/cmip6-dkrz/>], ICOS (2019) [datasets accessible at <https://hdl.handle.net/11676/0WzAlJkSQDK2YuLXnkw6BX> and <https://hdl.handle.net/11676/jGBBiZrsgz19J47noGGPzpPj>], Jackowicz-Korczynski et al., (2010) [data included in the paper, <https://doi.org/10.1029/2008JG000913>].

Observational data from Heliasz (2012), Christensen et al. 2012, and Finderup Nielsen et al. (2019), and that listed in the Supplementary material as A. Michelsen, not published,

M. Johansson, not published, and D. Pascual, not published, will be available in a repository (<https://dataguru.lu.se/> or PANGAEA) by the time the article is accepted.

The output data is available in the supporting information, figures, and/or tables, during peer review, and will be deposited to (<https://dataguru.lu.se/> or PANGAEA) by the time the article is accepted.

References

- Abisko Scientific Research Station, 2020. Meteorological Data from Abisko Observatory, Daily Values 1913-01-01 – 2020-12-31. [dataset available upon request]
- Amap, 2021. Arctic Climate Change Update 2021: Key Trends and Impacts. Summary for Policy-Makers. Arctic Monitoring and Assessment Programme (AMAP), p. 16. Tromsø, Norway.
- Batjes, N.H., 2012. ISRIC-WISE derived soil properties on a 5 by 5 arc-minute global grid (Ver. 1.2). Report 2012/01, ISRIC – World Soil Information, Wageningen (with data set, available at www.isric.org) Report 2012/01. 52 pp.; 9 fig.; 6 tab.; 48 ref.

Bartsch, A., Kumpula, T., Forbes, B., Stammeler, F., 2010. Detection of snow surface thawing and refreezing in the Eurasian Arctic using QuikSCAT: implications for reindeer herding. *Ecol. Appl.*, 20, 2346–2358. <https://doi.org/10.1890/09-1927>.

Beer, C., Porada, P., Ekici, A., Brakebusch, M., 2018. Effects of short-term variability of meteorological variables on soil temperature in permafrost regions. *Cryosphere.*, 12, 741–757.

Belda, M.D., Anthoni, P., Wårlind, D., Olin, S., Schurgers, G., Tang, J., Smith, B., Arneth, A. 2022. LPJ-GUESS/LSMv1.0: A next generation Land Surface Model with high ecological realism, *Geosci. Model Dev.*, 15, 6709–6745, <https://doi.org/10.5194/gmd-2022-1>.

Bokhorst, S., Bjerke, J.W., Tømmervik, H., Callaghan, T.V., Phoenix, G.K., 2009. Winter warming events damage sub-Arctic vegetation: consistent evidence from an experimental manipulation and a natural event. *J. Ecol.*, 97: 1408–1415.

Bokhorst, S., Bjerke, J.W., Davey, M.P., Taulavuori, K., Taulavuori, E., Laine, K., Callaghan, T.V., Phoenix, J.K., 2010. Impacts of extreme winter warming events on plant physiology in a sub-Arctic heath community. *Physiol. Plant.*, 140: 128–140.

Bruhwyler, L., Parmentier, F.-J.W., Crill, P., Leonard, M., Palmer, P.I., 2021. The Arctic Carbon Cycle and Its Response to Changing Climate. *Curr. Clim. Change Rep.*, 7, 14.

Callaghan, T.V., Bergholm, F., Christensen, T.R., Jonasson, C., Kokfelt, U., Johansson, M., 2010. A new climate era in the sub-Arctic: Accelerating climate changes and multiple impacts. *Geophys. Res. Lett.*, 37: L14705.

Crank, J., Nicolson, P. 1996. A practical method for numerical evaluation of solutions of partial differential equations of the heat-conduction type, *Adv. Comput. Math.*, 6, 207–226, doi:10.1007/BF02127704.

Ed Dlugokencky and Pieter Tans, NOAA/GML (gml.noaa.gov/ccgg/trends/) [dataset]

Eyring, V., Bony, S., Meehl, G.A., Senior, C.A., Stevens, B., Stouffer, R. J., Taylor, K. E., 2016. Overview of the Coupled Model Intercomparison Project Phase 6 (CMIP6) experimental design and organization, *Geosci. Model Dev.*, 9, 1937–1958, <https://doi.org/10.5194/gmd-9-1937-2016>. [dataset accessible at <https://esgf-data.dkrz.de/search/cmip6-dkrz/>]

Hansen, B.B., Isaksen, K., Benestad, R.E., Kohler, J., Larsen, J.O., Varpe, Ø., Pedersen, Å. Ø., Loe, L.E., et al., 2014. Warmer and wetter winters: characteristics and implications of an extreme weather event in the High Arctic. *Environ. Res. Lett.*, 9, 114021 <https://doi.org/10.1088/1748-9326/9/11/114021>.

Heliasz, M. 2012. Spatial and temporal dynamics of subarctic birch forest carbon exchange, Doctoral, Department of Physical Geography and Ecosystems Science, Lund University Sweden, 132 pp.

Johansson, M., Callaghan, T.V., Bosio, J., Åkerman, J., Jackowicz-Korczynski, M., Christensen, T.R., 2013. Rapid responses of permafrost and vegetation to experimentally increased snow cover in sub-arctic Sweden. *Environ. Res. Lett.*, 8: 035025.

Langlois, A., Johnson, C.-A, Montpetit, B., Royer, A., Blukacz-Richards, E.A. Neave, E. Dolant, C. Roy, et al., 2017. Detection of rain-on-snow (ROS) events and ice layer formation using passive microwave radiometry: A context for Peary caribou habitat in the Canadian Arctic, *Remote Sens Environ.*, 189, 84–95.

Michelsen, A., Rinnan, R., Jonasson, S., 2012. Two Decades of Experimental Manipulations of Heaths and Forest Understory in the Subarctic, *Ambio.*, 41, 218–230, doi:10.1007/s13280-012-0303-4.

Gustafson, A., Miller, P.A., Björk, R.G., Olin, S., 2021. Nitrogen restricts future sub-arctic treeline advance in an individual-based dynamic vegetation model, *Biogeosciences*, 18, 6329–6347, <https://doi.org/10.5194/bg-18-6329-2021>.

Natali, S.M., Watts, J.D., Rogers, B.M., Potter, S., Ludwig, S.M., Selbmann, A.-K., Sullivan, P.F., Abbott, B.W., et al., 2019. Large loss of CO₂ in winter observed across the northern permafrost region. *Nat. Clim. Chang.*, 9, <https://doi.org/10.1038/s41558-019-0592-8>, 2019.

Pan, C.G., Kirchner, P.B., Kimball, J.S., Kim, Y., Du, J., 2018. Rain-on-snow events in Alaska, their frequency and distribution from satellite observations. *Environ. Res. Lett.*, 13, 075004 <https://doi.org/10.1088/1748-9326/aac9d3>.

Pascual, D., Åkerman, J., Becher, M., Callaghan, T.V., Christensen, T.R., Dorrepaal, E., Emanuelsson, U., Giesler, R., et al., 2020. The missing pieces for better future predictions in subarctic ecosystems. *Ambio*, 50 (2), 375–392. <https://doi.org/10.1007/s13280-020-01381-1>.

Pascual, D., Johansson, M., 2022. Increasing impacts of extreme winter warming events on permafrost, *Weather. Clim. Extreme.*, 36, <https://doi.org/10.1016/j.wace.2022.100450>

Phoenix, G.K., Bjerke, J.W., 2016. Arctic browning: extreme events and trends reversing arctic greening. *Global Change Biol.*, 22, 2960–2962. <https://doi.org/10.1111/gcb.13261>.

Pongracz, A., Wårlind, D., Miller, P.A., Parmentier, F.-J.W., 2021. Model simulations of arctic biogeochemistry and permafrost extent are highly sensitive to the implemented snow scheme. *Biogeosciences*, 18, 5767–5787.

Sheffield, J., Goteti, G., Wood, E. F., 2006. Development of a 50-yr high-resolution global dataset of meteorological forcings for land surface modeling, [dataset] *J. Climate.*, 19 (13), 3088–3111. [dataset accessible at <http://hydrology.princeton.edu/>]

Simin, T., Tang, J., Holst, T., Rinnan, R., 2021. Volatile organic compound emission in tundra shrubs – Dependence on species characteristics and the near-surface environment, *Environ. Exp. Bot.*, 184, 104387.

Smith, B., Prentice, I.C., Sykes, M.T., 2001. Representation of vegetation dynamics in the modelling of terrestrial ecosystems: comparing two contrasting approaches within European climate space, *Glob. Ecol. Biogeogr.*, 10, 621–637, doi:10.1046/j.1466-822X.2001.t01-1-00256.x.

Smith, B., Wårlind, D., Arneth, A., Hickler, T., Leadley, P., Siltberg, J., Zaehle, S., 2014. Implications of incorporating N cycling and N limitations on primary production in an individual based dynamic vegetation model, *Biogeosciences*, 11, 2027–2054, doi:10.5194/bg-11-2027-2014.

Swedish meteorological, hydrological institute (SMHI). [dataset accessible at <https://www.smhi.se/data/utforskaren-oppna-data/?p=1&q=>]

Tang, J., Miller, P.A., Persson, A., Olefeldt, D., Pilesjö, P., Heliasz, M., Jackowicz-Korczynski, M., Yang, Z., et al., 2015. Carbon budget estimation of a subarctic catchment using a dynamic ecosystem model at high spatial resolution. *Biogeosciences*, 12: 2791–2808.

Van Bogaert R. 2010 Recent treeline dynamics in sub-Arctic Sweden: a multidisciplinary landscape assessment. Doctoral, Geography Department, Ghent University, Ghent.

Vikhamar-Schuler, D., Isaksen, K., Haugen, J.E., 2016. Changes in winter warming events in the nordic arctic region. *J. Clim.*, 29, 6223–6244.

Wania, R., Ross, I., Prentice, I. C., 2009. Integrating peatlands and permafrost into a dynamic global vegetation model; 1, Evaluation and sensitivity of physical land surface processes, *Global Biogeochem. Cy.*, 23, GB3014, doi:10.1029/2008gb003412.

Wania, R., Ross, I., Prentice, I. C. 2009. Integrating peatlands and permafrost into a dynamic global vegetation model; 2, Evaluation and sensitivity of vegetation and carbon cycle processes, *Global Biogeochem. Cy.*, 23, GB3015, doi:10.1029/2008gb003413.

Wania, R., Ross, I., Prentice, I. C. 2010. Implementation and evaluation of a new methane model within a dynamic global vegetation model: LPJ-WHyMe v1.3.1, *Geosci. Model Dev.*, 3, 565–584, doi:10.5194/gmd-3-565-2010.

Westermann, S., Boike, J., Langer, M., Schuler, T.V., Eitzelmüller, B., 2011. Modeling the impact of winter-time rain events on the thermal regime of permafrost. *Cryosphere*, 5, 945–959. <https://doi.org/10.5194/tc-5-945-2011>.

Zhang, T., 2005. Influence of the seasonal snow cover on the ground thermal regime: An overview. *Rev. Geophys.* 43(4).

References From the Supporting Information

Abisko Scientific Research Station, 2020. Meteorological Data from Abisko Observatory, Daily Values 1913-01-01 – 2020, pp. 12–31

Anderson, E. A. 1976. A point energy and mass balance model of a snow cover, NOAA technical report NWS 19., Md: Office of Hydrology, National Weather Service.

Best, M. J., Pryor, M., Clark, D. B., Rooney, G. G., Essery, R. L. H., Ménard, C. B., Edwards, J. M., Hendry, M. A., et al. 2011. The Joint UK Land 500 Environment Simulator (JULES), model description “ Part 1: Energy and water fluxes, *Geosci. Model Dev*, 4, 677–699, <https://doi.org/10.5194/gmd-4-677-2011>, 2011.

Christensen, T. R., Jackowicz-Korczyński, M., Aurela, M., Crill, P., Heliasz, M., Mastepanov, M., Friborg, T. 2012. Monitoring the Multi-Year Carbon Balance of a Subarctic Palsa Mire with Micrometeorological Techniques, *AMBIO*, 41, 207–217, doi:10.1007/s13280-012-0302-5.

D’Amboise, C. J. L., Müller, K., Oxarango, L., Morin, S., Schuler, T. V. 2017. Implementation of a physically based water percolation routine in the Crocus/SURFEX (V7.3) snowpack model, *Geosci. Model Dev.*, 10, 3547–3566, <https://doi.org/10.5194/gmd-10-3547-2017>, 2017.

Eyring, V., Bony, S., Meehl, G.A., Senior, C.A., Stevens, B., Stouffer, R. J., Taylor, K. E., 2016. Overview of the Coupled Model Intercomparison Project Phase 6 (CMIP6) experimental design and organization, *Geosci. Model Dev.*, 9, 1937–1958, <https://doi.org/10.5194/gmd-9-1937-2016>.

Finderup Nielsen T., Ravn N.R., Michelsen A. 2019. Increased CO₂ efflux due to long-term experimental summer warming and litter input in subarctic tundra – CO₂ fluxes at snowmelt, in growing season, fall and winter. *Plant Soil* 444:365-382 <https://doi.org/10.1007/s11104-019-04282-9>

Fukusako, S. 1990. Thermophysical Properties of Ice, Snow, and Sea Ice, *Int. J. Thermophys.*, 11.

Gutowski, W.J., Jr., Decker, S.G., Donavon, R.A., Pan, Z., Arritt, R.W., & Takle, E.S. 2003. Temporal–Spatial Scales of Observed and Simulated Precipitation in Central U.S. Climate, *J. Clim*, 16(22), 3841–3847.

Hawkins, E., Osborne, T.M., Ho, C.K., Challinor, A.J., 2013. Calibration and bias correction of climate projections for crop modelling: An idealised case study over Europe, *Agric. For. Meteorol.*, 170, 19–31.

Heliasz, M. 2012. Spatial and temporal dynamics of subarctic birch forest carbon exchange, Doctoral, Department of Physical Geography and Ecosystems Science, Lund University Sweden, 132 pp.

Jackowicz-Korczyński, M., Christensen, T. R., Bäckstrand, K., Crill, P., Friborg, T., Mastepanov, M., Ström, L. 2010. Annual cycle of methane emission from a subarctic peatland, *J. Geophys. Res.-Biogeo.*, 115, G02009, doi:10.1029/2008JG000913.

Pappas, C., Fatichi, S., Leuzinger, S., Wolf, A., Burlando, P. 2013. Sensitivity analysis of a process-based ecosystem model: Pinpointing parameterization and structural issues, *J. Geophys. Res.-Biogeo.*, 118, 505–528, doi:10.1002/jgrg.20035.

Pascual, D., Johansson, M., 2022. Increasing impacts of extreme winter warming events on permafrost, *Weather. Clim. Extreme*, 36, <https://doi.org/10.1016/j.wace.2022.100450>.

- Riahi, K., van Vuuren, D.P, Kriegler, E., Edmonds, j., O’Neill, B.C., Fujimori, S., Bauer, N., Calvin, K., et al., 2017. The Shared Socioeconomic Pathways and their energy, land use, and greenhouse gas emissions implications: An overview, *Glob. Environ. Change.*, 42, 153–168, doi.org/10.1016/j.gloenvcha.2016.05.009.
- Rinne, J., Swedish National Network, 2019. Ecosystem fluxes time series (ICOS Sweden), Abisko-Stordalen Palsa Bog, 2015-12-31–2016-12-31, [dataset] https://hdl.handle.net/11676/0WzAlJkSQDK2YuLXnkW6BX_
- Rinne, J., Swedish National Network, 2019. Ecosystem fluxes time series (ICOS Sweden), Abisko-Stordalen Palsa Bog, 2016-12-31–2017-12-31, [dataset] <https://hdl.handle.net/11676/jGBBiZrsgz19J47noGgPzpPf>
- Saltelli, A. 2002. Making best use of model evaluations to compute sensitivity indices, *Comput. Phys. Commun.*, 145(2), 280–297, doi:10.1016/S0010-4655(02)00280-1.
- Saltelli, A., Ratto, M., Andres, T., Campolongo, F., Cariboni, J., Gatelli, D., Saisana, M., & Tarantola, S. 2008. *Global Sensitivity Analysis: The Primer*, Wiley-Blackwell, Chichester.
- Saltelli, A., & Annoni, P. 2010. How to avoid a perfunctory sensitivity analysis, *Environ. Model. Software*, 25(12), 1508–1517, doi:10.1016/j.envsoft.2010.04.012.
- Sheffield, J., Goteti, G., Wood, E. F., 2006. Development of a 50-yr high-resolution global dataset of meteorological forcings for land surface modeling, *J. Climate*, 19 (13), 3088-3111.
- Singh, P., Spitzbart, G., Hübl, H., Weinmeister, H.W. 1997. Hydrological response of snowpack under rain-on-snow events: a field study, *J. Hydrol*, 202, (1–4). 1–20, [https://doi.org/10.1016/S0022-1694\(97\)00004-8](https://doi.org/10.1016/S0022-1694(97)00004-8).
- Swedish meteorological, hydrological institute (SMHI). www.smhi.se/.
- Tang, J., Schurgers, G., Valolahti, H., Faubert, P., Tiiva, P., Michelsen, A., Rinnan, R., 2016. Challenges in modelling isoprene and monoterpene emission dynamics of Arctic plants: a case study from a subarctic tundra heath, *Biogeosciences*, 13, 6651–6667, <https://doi.org/10.5194/bg-13-6651-2016>.
- Vikhamar-Schuler, D., Isaksen, K., Haugen, J.E., 2016. Changes in winter warming events in the nordic arctic region. *J. Clim.* 29, 6223–6244.
- Vionnet, V., Brun, E., Morin, S., Boone, A., Faroux, S., Le Moigne, P., Martin, E., Willemet, J.-M. 2012. The detailed snowpack scheme Crocus and its implementation in SURFEX v7.2, *Geosci. Model Dev*, 5, 773–791, <https://doi.org/10.5194/gmd-5-773-2012>.

D. Pascual^{1*}, M. Johansson¹, A. Pongracz¹, & J. Tang^{1,2}

¹Department of Physical Geography and Ecosystem Science, Lund University, Lund Sweden

²Section of Terrestrial Ecology, Department of Biology, University of Copenhagen. Copenhagen, Denmark

*Corresponding author. E-mail: Didac.pascual@nateko.lu.se - Affiliation address: Sölvegatan 12, 223 62 Lund, Sweden - Telephone dir 0046 720324595

Key Points:

- Winter warming events (WWEs) have increased in the Arctic and are expected to increase further, but their impacts are not thoroughly evaluated in large-scale ecosystem models.
- We applied different scenarios of enhanced WWEs in a widely used ecosystem model, LPJ-GUESS, and found that their impacts on ecosystem processes could be substantial and of magnitudes comparable to those of altered winter climatologies.
- The direction of the modeled WWE impacts on ground temperatures differed from what the observation-based literature suggests, and we identified essential processes lacking in LPJ-GUESS that may cause this mismatch.

Abstract

Winter warming events (WWEs) are short-lasting events of unusually warm weather, occasionally combined with rainfall, which can cause severe ecosystem impacts by altering ground temperatures and water fluxes. These impacts are generally overlooked in large-scale ecosystem models. The frequency and intensity of WWEs will likely increase further in the future. We used an ecosystem model, LPJ-GUESS, to investigate the responses of four subarctic ecosystems to different levels of predicted WWEs, and identify model gaps hindering accurate estimates of these responses. In response to WWEs, the model simulated substantial ground cooling (up to 2 °C in winter) in contrast to the observed warming, leading to changes in biogeochemical fluxes often comparable in magnitude to those from altered winter climatologies. The mismatch between the modelled and the observed ground temperature changes may be due to the 1) lacking surface energy balance, 2) daily timestep, and 3) simplistic water retention scheme in LPJ-GUESS.

Plain Language Summary

In the Arctic, winter warming events (WWEs) are episodes of exceptionally warm weather that last from hours to a few days and often occur in combination with rainfall. The combined effect of multiple processes triggered by WWEs (involving, for example, changes in snow depth and snow properties,

and heat exchanges between air, rain and meltwater, and soils) results in profound changes in ground temperatures and water fluxes, which many ecosystem processes depend on (vegetation dynamics, organic matter decomposition by microbes, etc). However, large-scale ecosystem models, which are used to study how arctic ecosystems will change in the future, often overlook the effects of WWEs because they oversimplify some complex physical processes and operate at longer temporal scales than WWEs. WWEs will likely become more frequent and intense in the future as the climate continues to warm. This study used a widely used ecosystem model, LPJ-GUESS, to investigate how the ecosystems will respond to more frequent and intense WWEs. The ecosystem responses that we observed were notable but in the opposite direction as observed in field measurements. We identified the processes that are lacking in the model and are causing this mismatch which, if implemented in the model, would significantly improve the predictions of future ecosystem changes in response to climate change.

1 Introduction

The Arctic is warming three times faster than the global average, with the strongest warming occurring in autumn and winter (AMAP 2021). The occurrence and impacts of winter warming events (WWEs), i.e. short-lasting extraordinarily warm spells, often accompanied by rainfall (rain on snow; ROS), are increasing rapidly and expanding geographically (e.g. Bartsch et al., 2010; Vikhamar-Schuler et al., 2016; Pan et al., 2018). Climate models predict a further increase in the coming decades. Despite their short duration, these extreme events could cause societal and environmental impacts that can override the impacts of long-term climatic trends (e.g., Phoenix & Bjerke, 2016).

In the winter, the impacts of WWEs are currently considered a research priority for better understanding future ecosystem dynamics in the subarctic (Pascual et al., 2020). WWEs can affect ground temperatures (GT) in multiple ways, mostly through: (1) direct heat transfer from the air, (2) latent heat release from refreezing melt and rainwater, and (3) changing the snowpack properties, such as depth and density, which influence the energy exchanges between the atmosphere, snow, and soil. These altered winter processes can further influence ground albedo and groundwater content (GWC), which has impacts lasting to the growing seasons (Pascual & Johansson, 2022). These WWE-associated environmental changes can further alter microbial activity, greenhouse gas (GHG) emissions (e.g., Natali et al., 2019), and permafrost and vegetation dynamics (Bruhwiler et al., 2021), ultimately altering the arctic carbon budget.

These interlinked processes and feedbacks related to WWEs are difficult to disentangle in observational data and thus challenging to implement in models. Moreover, large-scale ecosystem models which run with monthly climate data do not explicitly account for the impacts of such stochastic climate extremes (e.g. Tang et al., 2015).

In this study, we investigate the potential effects of predicted WWE scenarios

on winter and growing-season physical and biogeochemical variables using the latest version of a widely used dynamic ecosystem model, LPJ-GUESS. We aim to evaluate the model’s performance and identify model gaps in representing ecosystem responses to future WWEs.

2 Materials and Methods

2.1 Study sites

The Torneträsk area, in northern Sweden, is a topographically heterogeneous area that aligns along a strong west-east oceanic-continental climatic gradient, with precipitation and winter temperature decreasing eastwards due to the increasing continentality and the rain shadow effect caused by the Scandes Mountains. The area has experienced rapid climate warming (Callaghan et al., 2010) and a substantial increase in the frequency and intensity of WWEs (Pascual & Johansson, 2022).

Vegetation in the area varies following its climatic and altitudinal gradients. Birch forests occur below c. 600 and 800 m.a.s.l (Van Bogaert, 2010). Tundra species dominate above the tree-line, while in the lowlands, birch forests alternate with peat plateaus underlain by permafrost, and non-permafrost fens.

In this modelling study, we selected four sites representing these dominant ecosystem types in the Torneträsk area, including (1) a birch forest (~370 m.a.s.l) located <10 km east of the Abisko Station (ANS) (Heliasz et al., 2012); (2) a tundra site (~410 m.a.s.l), located <1 km to the southeast of the ANS (Michelsen et al., 2012 and references therein); (3) a peat plateau (~380 m.a.s.l) known as Storflaket, located c. 6 km east of the ANS (Johansson et al., 2013), and (4) a fen (~515 m.a.s.l) located c. 25 km west of the ANS, near the Katterjokk Station (SMHI). The dominant vegetation species at these sites are found in Appendix A.

2.2 Model description and simulation setup

2.2.1 Model description

The Lund-Potsdam-Jena General Ecosystem Simulator (LPJ-GUESS) is a process-based dynamic ecosystem model widely used on regional and global scale studies (Smith et al., 2001; 2014). The model simulates vegetation dynamics (including vegetation establishment, mortality and competition, etc.), water, carbon and nitrogen cycles, and soil biogeochemistry. This study used the latest version of LPJ-GUESS (version 4.1, Smith et al., 2014), with the recently-developed dynamic, intermediate complexity snow scheme enabling the simulation of climate-snow-soil interaction. The model can simulate up to five snow layers, their physical and thermal properties, and their development throughout the cold season. Based on the individual snow layer properties (e.g., temperature, density, thermal conductivity), freeze-thaw processes in snow layers, and heat transport through the snowpack between the atmosphere and soil can be simulated, and ROS events can be accounted for (Pongracz et al., 2021). LPJ-GUESS includes detailed representations of permafrost and

wetland processes, including peatland hydrology, peatland-specific PFTs, and CH₄ emissions (see Wania et al., 2009a, 2009b, 2010).

2.2.2 Model setup

Daily climate data provided by the ANS (ANS 2020) and Katterjokk Station (SMHI), including air temperature, air temperature daily range, and precipitation, together with shortwave radiation (1913-1984, Sheffield et al., 2006; 1984-2018, ANS) and annual CO₂ concentrations obtained from the Global Monitoring Laboratory (<https://gml.noaa.gov/ccgg/trends/>), were used to drive the model from 1913 to 2018. Soil property data was extracted from the WISE5min, V1.2 Soil Property Database (Batjes 2012). More details about the setup and input data are found in Appendix B.

Representative plant functional types (PFTs) were selected for each site (Table A1). We enabled high-latitude and wetland-specific plant functional types (PFTs) in the simulations to better capture site-specific vegetation conditions (see Wania et al., 2009 for more details). The PFT parameters at each site followed previous studies (e.g., Tang et al., 2015; Gustafson et al., 2021) (Table A2).

2.2.3 Model calibration and evaluation

Sobol sensitivity analyses (SA) were conducted to explore the influence of different parameters and parameter interactions on the estimated seasonal snow density, snow depth, snow temperature, and GT at the study sites (except for the tundra site due to lack of observational data for calibration and evaluation) (Appendix D). A sampling of eight relevant parameters, using ranges based on literature values, and a certain percentage of changes from the original values (Table D1), was conducted. Among the most influential parameters, we selected the parameter values that minimized the absolute differences between the measured and the modeled seasonal snow depth and GT at each site (2006-2012 at the peat plateau, 2001-2010 elsewhere) (Figures D4-8). The model was subsequently evaluated with independent observational data (2011-2018) when possible (Appendix E).

2.2.4 Model simulations with future WWEs

We generated manipulation experiments with different levels of WWE frequencies and intensities imposed on the observation-based climate inputs (HISTORICAL dataset) to assess the responses of different ecosystem processes to these extreme events. The applied frequencies and intensities were based on different climate scenarios in the Coupled Model Intercomparison Project Phase 6 (CMIP6) (Eyring et al., 2016). We selected six climate scenarios from two general circulation models (GCMs) with different climate sensitivities, i.e., CanESM5 and GFDL-ESM4, and three shared socioeconomic pathways representing three levels of varying GHG projections, i.e., SSP119, SSP270, and SSP585. For each scenario (n=6), daily meteorological data (1950-2100) for the gridcell near the Torneträsk area was extracted, and then bias-corrected at a daily scale. De-

tailed descriptions of the CMIP6 scenarios and the bias-correction method are found in Appendix C.

The bias-corrected GCM’s outputs were used to create the manipulation experiments (Table 1). In addition to the HISTORICAL runs (S0), we designed three additional experiments in which the future monthly anomalies in the frequency and intensity of melt days (S1), ROS (S2), and both (S3) in the GCM’s outputs (Table C2) were added to the HISTORICAL climate inputs, maintaining the long-term climate means as unchanged as possible. These anomalies were calculated based on four indices modified from Vikhamar et al. (2016) (Table C1).

The effects of altered WWEs and those from the altered long-term climate trends were compared by using an additional experiment (S4) in which the future winter monthly anomalies (Table C3) were directly added to the historical daily air temperature and precipitation.

Table 1. *Description of the HISTORICAL and MANIPULATION runs.*

Simulation names	Description
S0	HISTORICAL scenario
S1	Altered melt days frequency (WWE index 1 = n days with $T > 0^\circ$) and intensity (WWE index 2 = n days with $T > 0^\circ$ and $P > 1$ mm)
S2	Altered ROS frequency (WWE index 3 = n days with $T > 0^\circ$, and $P > 1$ mm) and intensity (WWE index 4 = n days with $T > 0^\circ$ and $P > 1$ mm)
S3	Altered frequency and intensity of both melt days and ROS (indices 1, 2, 3 & 4)
S4	Altered winter climatologies

Note. T and P refer to air temperature and precipitation. The monthly anomalies were calculated for November to March based on periods of 2071-2100 and 1985-2014.

3 Results and discussion

3.1 Sensitivity analyses and model calibration

The Sobol indices showed that the dens_min (minimum snow density) and compaction_rate (the rate at which snow is compacted over time), and their interactions, mainly influence the modelled seasonal snow depth, snow density, snow temperature, and GT (Figure D1-3).

The parameter values yielding the lowest measured-modelled differences in seasonal snow depth and GT are 50, 60, and 90 for dens_min, and 0.5, 0.8, and 0.9, for compaction_rate, at the birch forest, peat plateau, and fen sites, respectively (Figure D4-8).

For the tundra site, we applied parameter values of 90 and 0.8 for minimum snow density and compaction rate, as these showed the best agreement with the available growing-season observational data.

3.2 Evaluation of physical and biogeochemical variables in the historical period

3.2.1 Evaluation of physical variables

The seasonal patterns of snow cover were captured in the model at all sites. However, snowpack depth was considerably underestimated at the birch forest and the low-elevated fen site, but overestimated in low vegetation settings such as the peat plateau (Figure E1), likely due to the model lacking lateral transport and trapping/deposition of wind-blown snow. This mismatch affected the snow insulating capacity and caused substantial cold and warm biases in winter GT in the birch forest and peat plateau, respectively, but not in the fen (Figure E2) where the modelled snowpack depth exceeds the depth of the maximum insulating effect (40 cm; Zhang, 2005). The growing season GT was well captured at the birch forest and fen sites, but was underestimated in the peat plateau (Figure E2a,c,d).

The model was able to simulate short-term fluctuations in snow depth and GT during WWEs at all sites, but not their magnitudes (Figure E3). At the birch forest and peat plateau, larger than measured fluctuations in GT were modeled during WWEs and these differences were much smaller in the late winters. The modelled differences were largely linked to the simulated insulating capacity of snowpacks. Noticeably, stronger modeled reductions in snow depth occurred during early- and mid-winter WWEs, when the energy needed to warm-up and subsequently melt the thin and fresh (less dense) snowpacks is smaller. The modeled and measured GTs at the fen site remained around 0 °C throughout the winter due to the strong insulation of the thick snowpack, but the model captured the observed snowpack responses to WWEs.

3.2.2 Evaluation of biogeochemical variables

The modeled maximum LAI of 1.6 and 1.5 fell within the observed ranges at the birch forest (Heliasz, 2012) and tundra sites (Simin et al., 2021). Following the biases in GT, winter CO₂ heterotrophic respiration (R_h) was underestimated at the birch forest and overestimated at the peat plateau (Figure E4). We speculate an overestimation of winter R_h at the tundra –it presents similar winter R_h values than the fen and peat plateau, and 6-fold larger than the birch forest– due to the overestimated soil C pool at this site. The model underestimated the growing-season ecosystem respiration (R_{eco}) and gross primary production (GPP) in the tundra (Figure E5c,d). At the birch forest, the model predicted a strong annual C sink in 2007-2010, but measurements indicated a fairly neutral C balance (Figure E4a,b). At the peat plateau and fen sites, the model captured the annual fluctuations and magnitudes of CO₂ fluxes (Figure E4c-f). Across four sites the model was unable to capture the observed strong C source in September.

The differences in CH₄ fluxes between the peat plateau and fen sites were well captured by the model. However, the model underestimated by 55% the winter CH₄ fluxes at the peat plateau, likely due to the colder bias in modeled GT (Figure E6a,b).

3.3 Effects of enhanced WWEs

3.3.1 Impacts on physical variables

The WWE experiments (S1-S3) caused an overall reduction in winter GT (up to 2 °C) in all ecosystem types, except for the runs driven by WWEs from CanESM5 SSP585 at the tundra and the peat plateau (Figure 1a-d). The modeled snow depth also decreased substantially under all WWE experiments. This might suggest that the major driver of the modelled WWE effects on winter GT is snow insulation, which decreases as a combination of the snowpack depth reduction, and the increased thermal diffusivity (caused by higher thermal conductivity and lower heat capacity after freeze-thaw processes), facilitating the heat exchange between atmosphere and soil (Figure 3). However, a “tipping point” may be crossed above a certain WWE magnitude, when the strong cooling effects of the reduced snow insulating capacity are counteracted by the stronger warming effects of longer and more extreme WWEs. This point is reached faster under shallow snowpacks where snow insulation is weak and its further reduction has a smaller effect on GT compared to the overall warmer conditions.

In contrast to WWEs, altered future winter climatologies (S4) increased the modeled winter GT at all sites, from less than 1 °C to as much as 4 °C at the birch forest, tundra, and peat plateau in the warmest scenario, i.e., CanESM5 SSP585, despite snowpack reductions of >80%. The modeled GT warming effect diminishes under thick snowpacks, due to the snow insulation-related process described above: at the fen site (thickest snowpack) we can only see a GT warming under CanESM5 SSP585.

Our results agree with the modelling results by Beer et al., (2018), who suggested that WWEs may cause GT cooling mainly by reducing the snowpack depth. However, there is increasing observational evidence that intense ROS events cause substantial and long-lasting GT warming in winter (e.g., Hansen et al., 2014) through the latent heat released from refreezing of infiltrated water at the bottom of thick snowpacks (Westermann et al., 2011; Pascual et al., 2022). This long-lasting GT warming cannot be captured in LPJ-GUESS due to the lack of essential processes describing the energy and water exchanges between the atmosphere, snowpack, and soil (Figure 3).

In non-winter, the impacts of the manipulation experiments on GT followed those seen for winter GT, although smaller in magnitude (Figure 1e-h). The WWE impacts on non-winter GWC (0-50 cm depth) were marginal except for the fen site (decrease of up to $0.3 \text{ m}^{-3} \text{ m}^{-3}$) (Figure F1). GWC affects the thermal properties of soils, and its reduction likely contributed to the larger non-winter GT cooling modeled at the fen. The reduced albedo following an earlier snow cover disappearance can contribute to faster GT warming in spring, but this process is not represented in the current version of LPJ-GUESS.

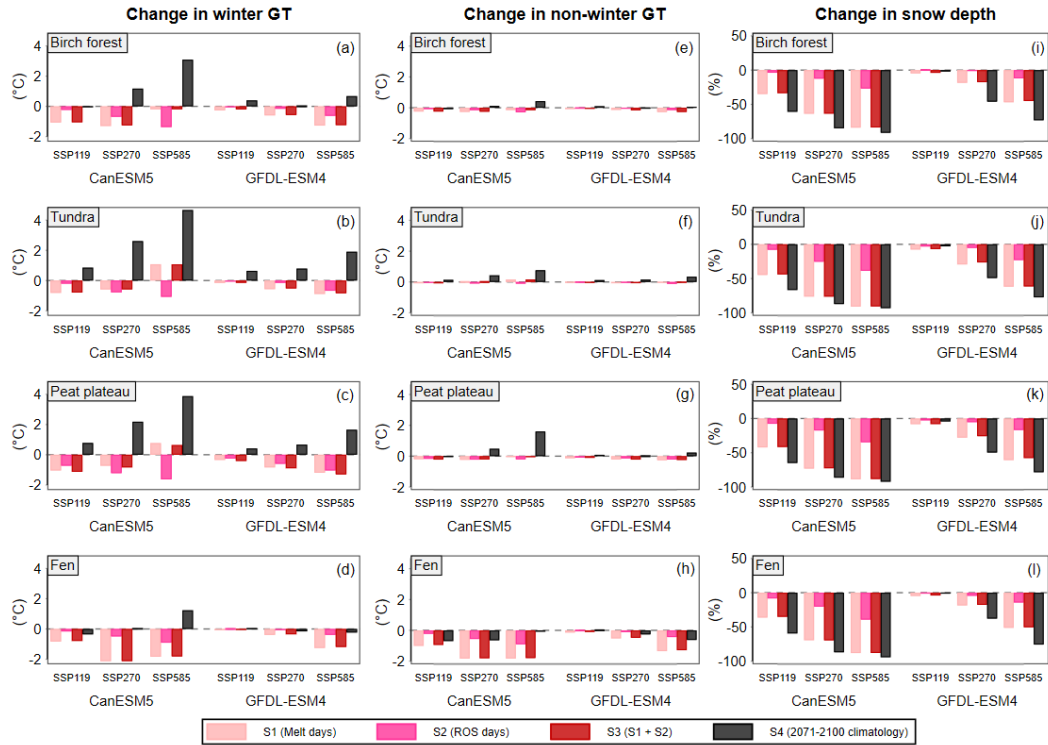


Figure 1. Differences between the MANIPULATION runs (S1-S4) and the HISTORICAL runs (S0) for winter GT ($^{\circ}\text{C}$; left column), non-winter GT ($^{\circ}\text{C}$; middle column), and winter snow depth (%; right column), at each site.

3.3.2 Impacts on biogeochemical variables

Our results further showed large WWE-induced impacts on all biogeochemical variables, with magnitudes often comparable to impacts deriving from altered winter climatologies (Figures 2 and G3). GT and water availability are key drivers of the ecosystem C cycle, as they influence the start of the growing season, nutrient availability, vegetation dynamics, and soil R_h .

The modelled impacts of the manipulation experiments on biogeochemical variables generally followed the same direction as those observed for GT and GWC. We noted substantial reductions in GPP (Figure 2i-l) under the WWE experiments S1 and S3 of up to 25% at the fen, 20% at the peat plateau, and 10% at the birch site, and smaller reductions under ROS events alone (S2). The tundra site showed weaker reductions in GPP than the other sites, ranging from a few percent to up to 5% in the milder WWE experiments (driven by SSP119), and increases of up to 10% under CanESM5 SSP585. In contrast, for S4, the model simulated weak changes in GPP in the mildest CMIP6 scenarios, but sizable

increases in GPP in the CanESM5 SSP585: up to 75% in the peat plateau, c. 50% in the birch forest, c. 25% in the tundra, and c. 10% in the fen site. The impacts on R_a mirrored those described for GPP (Figure 2e-h). Noticeably, the relationship between GT, and both GPP and R_a , is not linear because the processes involved in plant dynamics are multiple and complex. For example, observational and manipulation studies have reported considerable vegetation damage, delays in bud phenology, and reductions in vegetation greenness due to phenological and frost stress following WWEs (Bokhorst et al., 2009, 2010). These impacts on vegetation are not explicitly represented in the model, as it does not yet take into account these winter/spring stress-related processes.

Increases in GT can stimulate microbial activity and accelerate litter and soil decomposition rates, resulting in increased R_h (Natali et al., 2019). Accordingly, winter R_h increased or decreased by <5% at the fen, and up to 25% at the tundra and peat plateau, following the GT responses (Figure G1). Contrastingly, in response to the CanESM5 SSP585 scenario at the birch forest site, despite the overall lower winter GT, winter R_h increased by up to >200%. This may be explained because the modeled winter R_h in the birch forest is very low (6 g C m⁻², compared to >30 g C m⁻² at the other sites), and even small increases in R_h during WWEs can result in substantial relative increases in winter emissions. A recent synthesis of in situ observations across the Arctic indicates that winter R_h accounts for a substantial portion of the arctic's annual C budget (Natali et al., 2019). Winter R_h alone currently offsets ~40% of the measured annual vegetation C uptake at our sites. Applying the winter R_h response curve to GT by Natali et al., (2019) (Q10 = 2.9), WWE-induced impacts on winter GT of the magnitudes reported here could change total winter R_h by up to 25%. Hence, realistically simulating the effects of WWEs on GT is important for improving estimates of GHG emissions in high latitudes.

The modelled CH₄ emissions at the peat plateau and fen sites decreased under all WWE experiments due to WWE-induced decreases in GT and GWC (Figure G2). At the fen site, emissions halved mostly due to lower water tables in the non-winter season.

Overall, the year-round ecosystem C exchange (i.e. NEE) of the birch forest, tundra, and peat plateau sites decreased (i.e., became a smaller C sink) considerably under most WWE experiments (Figure G3), generally between 20% and 50%, and up to 90% occasionally in the tundra site, due to larger reductions in vegetation C assimilation compared to the C losses from R_h . Contrastingly, NEE at the fen site increased weakly (i.e., became a stronger C sink), mostly due to large reductions in R_h . Noticeably, the changes in NEE caused by WWEs (S1-S3) are substantial and of similar magnitude to those caused by shifts in future winter climatologies (S4). This further indicates that WWEs, despite their short duration, may have the potential to induce changes in high-latitude ecosystem C cycling of magnitudes comparable to those induced by long-term climatic trends.

Given the observed discrepancies in modeled vs measured GT responses to

WWEs (section 3.2.1), the modeled impacts on ecosystems C fluxes reported here should not be interpreted as a direction prediction of future impacts of WWEs, but rather as a sensitivity test of the current model’s responses to altered levels of WWEs.

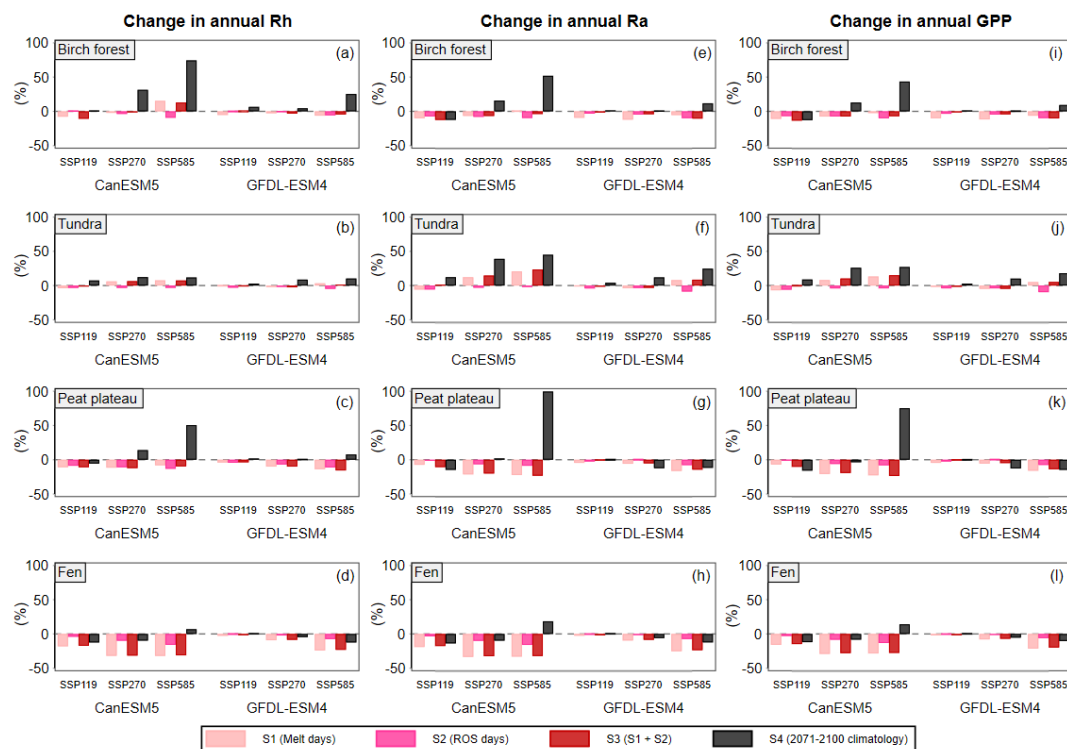


Figure 2. Differences between the MANIPULATION (S1-S4) and the HISTORICAL runs (S0), for annual Rh (%; left column), annual Ra (%; middle column), and annual GPP (%; right column), at each site.

3.4.3 Model limitations and potential developments

LPJ-GUESS has difficulties in capturing the physical changes in snow depth induced by WWEs. We identified the lack of surface energy balance in LPJ-GUESS as one of the main limitations to simulating WWE impacts on GT. Heat transfer between air-snow-soil layers is simulated using the Crank-Nicholson finite difference scheme (Crank and Nicolson, 1996). This indirect method of defining heat transfer may significantly affect the computed snow layer and ground temperatures, and the rate and magnitude of snowmelt events. Additionally, the model’s daily timestep may be too coarse to capture the sub-daily freeze-thaw cycles and hydrological processes within the snowpack.

In the model, heat transfer is affected by the changes in snow layer temperature

and thermal properties, and the latent heat release upon freezing is not captured (Figure 3). The SA showed that the current model setup is not sensitive to changes in liquid water holding capacity in snow layers (Figure D1-3), potentially due to the simplistic water retention scheme applied. Rainfall infiltration follows a bucket model approach, limited by each snow layer’s maximum water-holding capacity. Precipitation from ROS events and melt water is quickly forwarded to the soil as runoff at the simulated time step (i.e., daily) when the maximum liquid holding capacity of a layer is reached. If the ground is frozen, the excess liquid water will not stay in the bottom snow layer, but drain out as surface runoff. This feature also prevents the formation of ice layers of high thermal conductivity within the snow layers, as many observational studies suggest (e.g., Langlois et al., 2017), which could influence the simulated GT. Observations suggest major ROS events may have durable impacts on GT (e.g. Westermann et al., 2011), but the current model setup cannot capture such persistent effects due to the simple water retention scheme and the lacking processes related to energy balance.

The LPJ-GUESS version used in this study has an intermediate complexity snow scheme, similar to many ecosystem models. These modules are developed and tuned to represent average conditions rather than capturing extreme and smaller-scale phenomena such as WWEs. There is a need for either further snow scheme development in LPJ-GUESS or evaluating a more complex, designated snow model to address the listed shortcomings and capture internal snow dynamics on a finer spatio-temporal scale. A recent extension of the model with detailed land surface processes and surface energy balance LPJ-GUESS LSMv1.0 (Belda et al., 2022) could be used in future studies to assess whether the model-measurements mismatch is reduced when using the LPJ-GUESS with detailed energy balance and sub-daily processes. This land surface model version of LPJ-GUESS needs to be thoroughly evaluated and tested in high latitude environments. Regional modelling studies are required to further understand how WWEs might affect the pan-Arctic carbon budget.

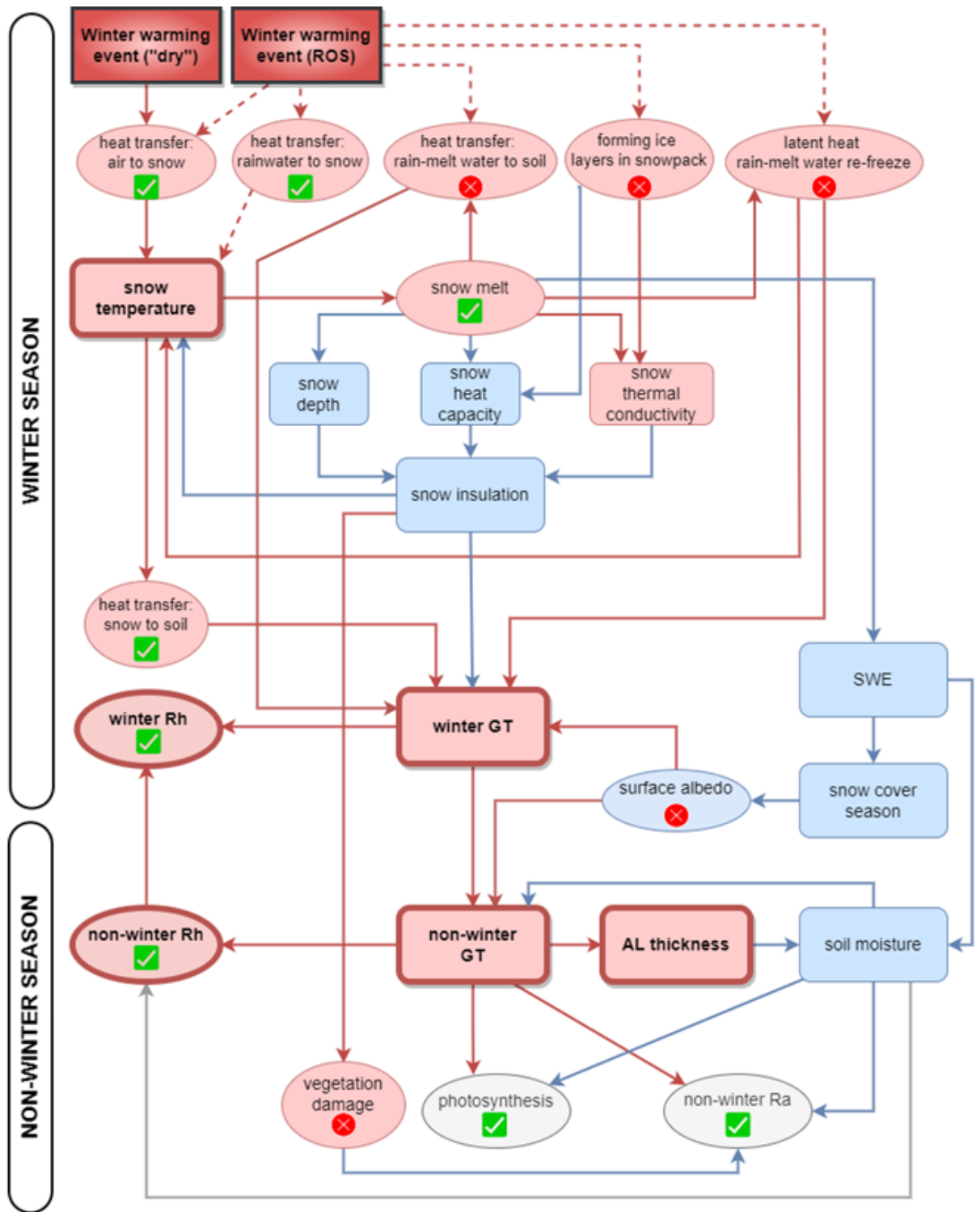


Figure 3. Theoretical model of the WWE impacts. Box colors indicate the overall direction of changes (red=increase, blue=decrease) in the variables based on the literature. Thick outlines and bold text indicate a disagreement between the literature and our simulations. Arrow colors show the direction of the change exerted by each process. Dashed lines refer to ROS-related processes. Grey boxes and lines refer to uncertain processes and responses. Green ticks and red crosses indicate WWE-related processes that are, or are not, implicitly implemented in the current model version.

5 Conclusions

We applied future-simulated WWE experiments in LPJ-GUESS to investigate the potential effects of these events on four dominant ecosystems in subarctic Sweden. The modeled impacts of WWEs on the ecosystem variables were substantial and of magnitudes often comparable to those of altered winter climatologies. These events induced reductions in GT which altered numerous biogeochemical processes and resulted in substantial changes in ecosystem CO₂ uptake. This highlights the need to realistically represent the effects of WWEs in ecosystem models -which are still largely overlooked especially in regional and large scale studies- to improve estimates of the current and future high-latitude C budget. The direction of the modeled impacts on GT differed from the majority of the observation-based literature. We identified the current model limitations contributing to this mismatch, including 1) the lack of surface energy balance, 2) the model's daily timestep, 3) and the simplistic water retention scheme applied in the LPJ-GUESS snow scheme.

Acknowledgments

Open access funding provided by Lund University. We are grateful to the Department of Physical Geography and Ecosystem Science, Lund University for the grant received to promote research integration and advancement of early-career researchers at the department 2018. We are also grateful to Anders Michelsen for valuable input. This study has been made possible by data provided by the Abisko Scientific Research Station and the Swedish Meteorological and Hydrological Institute (SMHI). J.T. is financially supported by Swedish FORMAS mobility grant (2016-01580) and acknowledges support from Lund University strategic research area Modelling the Regional and Global Earth System, MERGE. A.P acknowledges financial support from the Swedish Research Council (WinterGap, registration no. 2017-05268) and the Research Council of Norway (WINTERPROOF, project no. 274711).

Open Research

The code version used for this study is stored in a central code repository and will be made accessible upon request.

We provided the necessary descriptions for transparency and traceability of the analysis using our community standards.

Observational data used in this study can be retrieved from the following in-text data citation references: ANS (2020) [dataset, accessible upon request], SMHI (2020) [dataset accessible via <https://www.smhi.se/data/utforskaren-oppna-data/?p=1&q=>], Sheffield et al., (2006) [dataset available at <http://hydrology.princeton.edu/>], Global Monitoring Laboratory [dataset available at <https://gml.noaa.gov/ccgg/trends/>], Batjes et al., (2012) [dataset available at www.isric.org], Eyring et al., (2016) [dataset accessible at <https://esgf-data.dkrz.de/search/cmip6-dkrz/>], ICOS (2019) [datasets accessible at <https://hdl.handle.net/11676/0WzAlJikSQDK2YuLXnkW6BX> and <https://hdl.handle.net/11676/jGBBiZrsgz19J47noGGPzpPjf>], Jackowicz-Korczynski et al., (2010) [data included in the paper, <https://doi.org/10.1029/2008JG000913>].

Observational data from Heliasz (2012), Christensen et al. 2012, and Finderup Nielsen et al. (2019), and that listed in the Supplementary material as A. Michelsen, not published,

M. Johansson, not published, and D. Pascual, not published, will be available in a repository (<https://dataguru.lu.se/> or PANGAEA) by the time the article is accepted.

The output data is available in the supporting information, figures, and/or tables, during peer review, and will be deposited to (<https://dataguru.lu.se/> or PANGAEA) by the time the article is accepted.

References

- Abisko Scientific Research Station, 2020. Meteorological Data from Abisko Observatory, Daily Values 1913-01-01 – 2020-12-31. [dataset available upon request]
- Amap, 2021. Arctic Climate Change Update 2021: Key Trends and Impacts. Summary for Policy-Makers. Arctic Monitoring and Assessment Programme (AMAP), p. 16. Tromsø, Norway.
- Batjes, N.H., 2012. ISRIC-WISE derived soil properties on a 5 by 5 arc-minute global grid (Ver. 1.2). Report 2012/01, ISRIC – World Soil Information, Wageningen (with data set, available at www.isric.org) Report 2012/01. 52 pp.; 9 fig.; 6 tab.; 48 ref.
- Bartsch, A., Kumpula, T., Forbes, B., Stammer, F., 2010. Detection of snow surface thawing and refreezing in the Eurasian Arctic using QuikSCAT: implications for reindeer herding. *Ecol. Appl.*, 20, 2346–2358. <https://doi.org/10.1890/09-1927>.
- Beer, C., Porada, P., Ekici, A., Brakebusch, M., 2018. Effects of short-term variability of meteorological variables on soil temperature in permafrost regions. *Cryosphere.*, 12, 741–757.
- Belda, M.D., Anthoni, P., Wårilind, D., Olin, S., Schurgers, G., Tang, J., Smith,

- B., Arneth, A. 2022. LPJ-GUESS/LSMv1.0: A next generation Land Surface Model with high ecological realism, *Geosci. Model Dev.*, 15, 6709–6745, <https://doi.org/10.5194/gmd-2022-1>.
- Bokhorst, S., Bjerke, J.W., Tømmervik, H., Callaghan, T.V., Phoenix, G.K., 2009. Winter warming events damage sub-Arctic vegetation: consistent evidence from an experimental manipulation and a natural event. *J. Ecol.*, 97: 1408–1415.
- Bokhorst, S., Bjerke, J.W., Davey, M.P., Taulavuori, K., Taulavuori, E., Laine, K., Callaghan, T.V., Phoenix, J.K., 2010. Impacts of extreme winter warming events on plant physiology in a sub-Arctic heath community. *Physiol. Plant.*, 140: 128–140.
- Bruhwyler, L., Parmentier, F.-J.W., Crill, P., Leonard, M., Palmer, P.I., 2021. The Arctic Carbon Cycle and Its Response to Changing Climate. *Curr. Clim. Change Rep.*, 7, 14.
- Callaghan, T.V., Bergholm, F., Christensen, T.R., Jonasson, C., Kokfelt, U., Johansson, M., 2010. A new climate era in the sub-Arctic: Accelerating climate changes and multiple impacts. *Geophys. Res. Lett.*, 37: L14705.
- Crank, J., Nicolson, P. 1996. A practical method for numerical evaluation of solutions of partial differential equations of the heat-conduction type, *Adv. Comput. Math.*, 6, 207–226, doi:10.1007/BF02127704.
- Ed Dlugokencky and Pieter Tans, NOAA/GML (gml.noaa.gov/ccgg/trends/) [dataset]
- Eyring, V., Bony, S., Meehl, G.A., Senior, C.A., Stevens, B., Stouffer, R. J., Taylor, K. E., 2016. Overview of the Coupled Model Intercomparison Project Phase 6 (CMIP6) experimental design and organization, *Geosci. Model Dev.*, 9, 1937–1958, <https://doi.org/10.5194/gmd-9-1937-2016>. [*dataset accessible at <https://esgf-data.dkrz.de/search/cmip6-dkrz/>*]
- Hansen, B.B., Isaksen, K., Benestad, R.E., Kohler, J., Larsen, J.O., Varpe, Ø., Pedersen, Å. Ø., Loe, L.E., et al., 2014. Warmer and wetter winters: characteristics and implications of an extreme weather event in the High Arctic. *Environ. Res. Lett.*, 9, 114021 <https://doi.org/10.1088/1748-9326/9/11/114021>.
- Heliasz, M. 2012. Spatial and temporal dynamics of subarctic birch forest carbon exchange, Doctoral, Department of Physical Geography and Ecosystems Science, Lund University Sweden, 132 pp.
- Johansson, M., Callaghan, T.V., Bosio, J., Åkerman, J., Jackowicz-Korczynski, M., Christensen, T.R., 2013. Rapid responses of permafrost and vegetation to experimentally increased snow cover in sub-arctic Sweden. *Environ. Res. Lett.*, 8: 035025.
- Langlois, A., Johnson, C.-A., Montpetit, B., Royer, A., Blukacz-Richards, E.A. Neave, E. Dolant, C. Roy, et al., 2017. Detection of rain-on-snow (ROS) events

- and ice layer formation using passive microwave radiometry: A context for Peary caribou habitat in the Canadian Arctic, *Remote Sens Environ.*, 189, 84–95.
- Michelsen, A., Rinnan, R., Jonasson, S., 2012. Two Decades of Experimental Manipulations of Heaths and Forest Understory in the Subarctic, *Ambio.*, 41, 218–230, doi:10.1007/s13280-012-0303-4.
- Gustafson, A., Miller, P.A., Björk, R.G., Olin, S., 2021. Nitrogen restricts future sub-arctic treeline advance in an individual-based dynamic vegetation model, *Biogeosciences*, 18, 6329–6347, <https://doi.org/10.5194/bg-18-6329-2021>.
- Natali, S.M., Watts, J.D., Rogers, B.M., Potter, S., Ludwig, S.M., Selbmann, A.-K., Sullivan, P.F., Abbott, B.W., et al., 2019. Large loss of CO₂ in winter observed across the northern permafrost region. *Nat. Clim. Chang.*, 9, <https://doi.org/10.1038/s41558-019-0592-8>, 2019.
- Pan, C.G., Kirchner, P.B., Kimball, J.S., Kim, Y., Du, J., 2018. Rain-on-snow events in Alaska, their frequency and distribution from satellite observations. *Environ. Res. Lett.*, 13, 075004 <https://doi.org/10.1088/1748-9326/aac9d3>.
- Pascual, D., Åkerman, J., Becher, M., Callaghan, T.V., Christensen, T.R., Dorrepaal, E., Emanuelsson, U., Giesler, R., et al., 2020. The missing pieces for better future predictions in subarctic ecosystems. *Ambio*, 50 (2), 375–392. <https://doi.org/10.1007/s13280-020-01381-1>.
- Pascual, D., Johansson, M., 2022. Increasing impacts of extreme winter warming events on permafrost, *Weather. Clim. Extreme.*, 36, <https://doi.org/10.1016/j.wace.2022.100450>
- Phoenix, G.K., Bjerke, J.W., 2016. Arctic browning: extreme events and trends reversing arctic greening. *Global Change Biol.*, 22, 2960–2962. <https://doi.org/10.1111/gcb.13261>.
- Pongracz, A., Wårlind, D., Miller, P.A., Parmentier, F.-J.W., 2021. Model simulations of arctic biogeochemistry and permafrost extent are highly sensitive to the implemented snow scheme. *Biogeosciences*, 18, 5767–5787.
- Sheffield, J., Goteti, G., Wood, E. F., 2006. Development of a 50-yr high-resolution global dataset of meteorological forcings for land surface modeling, [dataset] *J. Climate.*, 19 (13), 3088–3111. [dataset accessible at <http://hydrology.princeton.edu/>]
- Simin, T., Tang, J., Holst, T., Rinnan, R., 2021. Volatile organic compound emission in tundra shrubs – Dependence on species characteristics and the near-surface environment, *Environ. Exp. Bot.*, 184, 104387.
- Smith, B., Prentice, I.C., Sykes, M.T., 2001. Representation of vegetation dynamics in the modelling of terrestrial ecosystems: comparing two contrasting approaches within European climate space, *Glob. Ecol. Biogeogr.*, 10, 621–637, doi:10.1046/j.1466-822X.2001.t01-1-00256.x.

Smith, B., Wårlind, D., Arneth, A., Hickler, T., Leadley, P., Siltberg, J., Zaehle, S., 2014. Implications of incorporating N cycling and N limitations on primary production in an individual based dynamic vegetation model, *Biogeosciences*, 11, 2027–2054, doi:10.5194/bg-11-2027-2014.

Swedish meteorological, hydrological institute (SMHI). [dataset accessible at <https://www.smhi.se/data/utforskaren-oppna-data/?p=1&q=>]

Tang, J., Miller, P.A., Persson, A., Olefeldt, D., Pilesjö, P., Heliasz, M., Jackowicz-Korczynski, M., Yang, Z., et al., 2015. Carbon budget estimation of a subarctic catchment using a dynamic ecosystem model at high spatial resolution. *Biogeosciences*, 12: 2791–2808.

Van Bogaert R. 2010 Recent treeline dynamics in sub-Arctic Sweden: a multidisciplinary landscape assessment. Doctoral, Geography Department, Ghent University, Ghent.

Vikhamar-Schuler, D., Isaksen, K., Haugen, J.E., 2016. Changes in winter warming events in the nordic arctic region. *J. Clim.*, 29, 6223–6244.

Wania, R., Ross, I., Prentice, I. C., 2009. Integrating peatlands and permafrost into a dynamic global vegetation model; 1, Evaluation and sensitivity of physical land surface processes, *Global Biogeochem. Cy.*, 23, GB3014, doi:10.1029/2008gb003412.

Wania, R., Ross, I., Prentice, I. C. 2009. Integrating peatlands and permafrost into a dynamic global vegetation model; 2, Evaluation and sensitivity of vegetation and carbon cycle processes, *Global Biogeochem. Cy.*, 23, GB3015, doi:10.1029/2008gb003413.

Wania, R., Ross, I., Prentice, I. C. 2010. Implementation and evaluation of a new methane model within a dynamic global vegetation model: LPJ-WHyMe v1.3.1, *Geosci. Model Dev.*, 3, 565–584, doi:10.5194/gmd-3-565-2010.

Westermann, S., Boike, J., Langer, M., Schuler, T.V., Eitzelmüller, B., 2011. Modeling the impact of wintertime rain events on the thermal regime of permafrost. *Cryosphere*, 5, 945–959. <https://doi.org/10.5194/tc-5-945-2011>.

Zhang, T., 2005. Influence of the seasonal snow cover on the ground thermal regime: An overview. *Rev. Geophys.* 43(4).

References From the Supporting Information

Abisko Scientific Research Station, 2020. Meteorological Data from Abisko Observatory, Daily Values 1913-01-01 – 2020, pp. 12–31

Anderson, E. A. 1976. A point energy and mass balance model of a snow cover, NOAA technical report NWS 19., Md: Office of Hydrology, National Weather Service.

Best, M. J., Pryor, M., Clark, D. B., Rooney, G. G., Essery, R. L. H., Ménard, C. B., Edwards, J. M., Hendry, M. A., et al. 2011. The Joint UK Land

500 Environment Simulator (JULES), model description “ Part 1: Energy and water fluxes, *Geosci. Model Dev*, 4, 677–699, <https://doi.org/10.5194/gmd-4-677-2011>, 2011.

Christensen, T. R., Jackowicz-Korczyński, M., Aurela, M., Crill, P., Heliasz, M., Mastepanov, M., Friborg, T. 2012. Monitoring the Multi-Year Carbon Balance of a Subarctic Palsa Mire with Micrometeorological Techniques, *AMBIO*, 41, 207–217, doi:10.1007/s13280-012-0302-5.

D’Amboise, C. J. L., Müller, K., Oxarango, L., Morin, S., Schuler, T. V. 2017. Implementation of a physically based water percolation routine in the Crocus/SURFEX (V7.3) snowpack model, *Geosci. Model Dev.*, 10, 3547–3566, <https://doi.org/10.5194/gmd-10-3547-2017>, 2017.

Eyring, V., Bony, S., Meehl, G.A., Senior, C.A., Stevens, B., Stouffer, R. J., Taylor, K. E., 2016. Overview of the Coupled Model Intercomparison Project Phase 6 (CMIP6) experimental design and organization, *Geosci. Model Dev.*, 9, 1937–1958, <https://doi.org/10.5194/gmd-9-1937-2016>.

Finderup Nielsen T., Ravn N.R., Michelsen A. 2019. Increased CO₂ efflux due to long-term experimental summer warming and litter input in subarctic tundra – CO₂ fluxes at snowmelt, in growing season, fall and winter. *Plant Soil* 444:365-382 <https://doi.org/10.1007/s11104-019-04282-9>

Fukusako, S. 1990. Thermophysical Properties of Ice, Snow, and Sea Ice, *Int. J. Thermophys.*, 11.

Gutowski, W.J., Jr., Decker, S.G., Donavon, R.A., Pan, Z., Arritt, R.W., & Takle, E.S. 2003. Temporal–Spatial Scales of Observed and Simulated Precipitation in Central U.S. Climate, *J. Clim.*, 16(22), 3841–3847.

Hawkins, E., Osborne, T.M., Ho, C.K., Challinor, A.J., 2013. Calibration and bias correction of climate projections for crop modelling: An idealised case study over Europe, *Agric. For. Meteorol.*, 170, 19–31.

Heliasz, M. 2012. Spatial and temporal dynamics of subarctic birch forest carbon exchange, Doctoral, Department of Physical Geography and Ecosystems Science, Lund University Sweden, 132 pp.

Jackowicz-Korczyński, M., Christensen, T. R., Bäckstrand, K., Crill, P., Friborg, T., Mastepanov, M., Ström, L. 2010. Annual cycle of methane emission from a subarctic peatland, *J. Geophys. Res.-Biogeo.*, 115, G02009, doi:10.1029/2008JG000913.

Pappas, C., Fatichi, S., Leuzinger, S., Wolf, A., Burlando, P. 2013. Sensitivity analysis of a process-based ecosystem model: Pinpointing parameterization and structural issues, *J. Geophys. Res.-Biogeo.*, 118, 505–528, doi:10.1002/jgrg.20035.

Pascual, D., Johansson, M., 2022. Increasing impacts of extreme winter warming events on permafrost, *Weather. Clim. Extreme*, 36, <https://doi.org/10.101>

6/j.wace.2022.100450.

Riahi, K., van Vuuren, D.P, Kriegler, E., Edmonds, j., O'Neill, B.C., Fujimori, S., Bauer, N., Calvin, K., et al., 2017. The Shared Socioeconomic Pathways and their energy, land use, and greenhouse gas emissions implications: An overview, *Glob. Environ. Change.*, 42, 153–168, doi.org/10.1016/j.gloenvcha.2016.05.009.

Rinne, J., Swedish National Network, 2019. Ecosystem fluxes time series (ICOS Sweden), Abisko-Stordalen Palsa Bog, 2015-12-31–2016-12-31, [dataset] https://hdl.handle.net/11676/0WzAlJlkSQDK2YuLXnkw6BX_

Rinne, J., Swedish National Network, 2019. Ecosystem fluxes time series (ICOS Sweden), Abisko-Stordalen Palsa Bog, 2016-12-31–2017-12-31, [dataset] <https://hdl.handle.net/11676/jGBBiZrsgz19J47noGGPzpPf>

Saltelli, A. 2002. Making best use of model evaluations to compute sensitivity indices, *Comput. Phys. Commun.*, 145(2), 280–297, doi:10.1016/S0010-4655(02)00280-1.

Saltelli, A., Ratto, M., Andres, T., Campolongo, F., Cariboni, J., Gatelli, D., Saisana, M., & Tarantola, S. 2008. *Global Sensitivity Analysis: The Primer*, Wiley-Blackwell, Chichester.

Saltelli, A., & Annoni, P. 2010. How to avoid a perfunctory sensitivity analysis, *Environ. Model. Software*, 25(12), 1508–1517, doi:10.1016/j.envsoft.2010.04.012.

Sheffield, J., Goteti, G., Wood, E. F., 2006. Development of a 50-yr high-resolution global dataset of meteorological forcings for land surface modeling, *J. Climate*, 19 (13), 3088-3111.

Singh, P., Spitzbart, G., Hübl, H ., Weinmeister, H.W. 1997. Hydrological response of snowpack under rain-on-snow events: a field study, *J. Hydrol*, 202, (1–4). 1–20, [https://doi.org/10.1016/S0022-1694\(97\)00004-8](https://doi.org/10.1016/S0022-1694(97)00004-8).

Swedish meteorological, hydrological institute (SMHI). www.smhi.se/.

Tang, J., Schurgers, G., Valolahti, H., Faubert, P., Tiiva, P., Michelsen, A., Rinnan, R., 2016. Challenges in modelling isoprene and monoterpene emission dynamics of Arctic plants: a case study from a subarctic tundra heath, *Biogeosciences*, 13, 6651–6667, <https://doi.org/10.5194/bg-13-6651-2016>.

Vikhamar-Schuler, D., Isaksen, K., Haugen, J.E., 2016. Changes in winter warming events in the nordic arctic region. *J. Clim.* 29, 6223–6244.

Vionnet, V., Brun, E., Morin, S., Boone, A., Faroux, S., Le Moigne, P., Martin, E., Willemet, J.-M. 2012. The detailed snowpack scheme Crocus and its implementation in SURFEX v7.2, *Geosci. Model Dev*, 5, 773–791, <https://doi.org/10.5194/gmd-5-773-2012>.

**Modelling the impacts of future enhanced winter warming events on subarctic ecosystem using
LPJ-GUESS**

D. Pascual^{1*}, M. Johansson¹, A. Pongracz¹, & J. Tang^{1,2}

¹Department of Physical Geography and Ecosystem Science, Lund University, Lund Sweden

²Section of Terrestrial Ecology, Department of Biology, University of Copenhagen. Copenhagen, Denmark

*Corresponding author. E-mail: Didac.pascual@nateko.lu.se - Affiliation address: Sölvegatan 12, 223 62 Lund, Sweden - Telephone dir 0046 720324595

Contents of this file

- A. Plant functional types (PFT's) simulated for the four modelled land cover types
- B. Input data
- C. WWE manipulation experiments
- D. Sensitivity analysis
- E. Model evaluation
- F. Impacts of WWE on physical variables
- G. Impacts of WWE on biogeochemical variables

Introduction

The Supporting information for this article contains the following information:

- A: a detailed description of the plant functional types and their parameterization.
- B: additional descriptions of the input data.
- C: detailed descriptions of the global climate model data used for the creation of the winter warming event scenarios, further details of the methods employed to create such scenarios, and an overview of the anomalies applied to create such scenarios.
- D: further details regarding the methods and the results of the Sensitivity Analysis.
- E: a list of the model evaluation data, and figures supporting the descriptions provided in the manuscript regarding the results of the model evaluation.
- F: additional figures to visualize the results of the study described in the main manuscript.

A. Plant functional types (PFT's) simulated for the four ecosystem types investigated

Table A1. Full details of the Plant Functional Types (PFTs) and typical species simulated in the different ecosystem types. Superscripts 1, 2, 3, and 4, denote each PFT belonging to the birch forest, tundra, peat plateau, and fen sites, respectively.

PFT name	Typical species
IBS ¹ (Shade-intolerant broadleaved summergreen tree)	<i>Betula pubescens</i>
LSE ^{1,2} (Low evergreen shrub)	<i>Empetrum hermaphroditum</i> , <i>Juniperus communis</i> , <i>Vaccinium vitis-idaea</i> ; <i>Andromeda polifolia</i>
LSS ² (Low summergreen shrub)	<i>Vaccinium myrtillus</i> , <i>V. uliginosum</i> , <i>Salix hastata</i> , <i>S. glauca</i> etc.
EPDS ² (Prostrate evergreen dwarf shrubs)	<i>Vaccinium oxycoccus</i> , <i>Cassiope tetragona</i> , <i>Dryas octopetala</i> , <i>Saxifraga oppositifolia</i>
SPDS ² (Prostrate summergreen dwarf shrub)	<i>Salix arctica</i> , <i>Arctostaphylos alpinus</i> , <i>Salix reticulata</i>
pLSE ³ (peatland low evergreen shrub)	<i>Vaccinium vitis-idaea</i> , <i>Cassiope tet.</i> ,
pLSS ³ (peatland low summergreen shrub)	<i>Vaccinium myrtillus</i> , <i>V. uliginosum</i> , <i>Salix hastata</i> , <i>S. glauca</i>
GRT ² (Graminoid and forb tundra)	<i>Artemisia</i> , <i>Kobresia</i> , <i>Brassicaceae</i>
CLM ^{1,2} (cushion forb, lichen and moss tundra)	<i>Saxifragaceae</i> , <i>Caryophyllaceae</i> , <i>Papaver</i> , <i>Draba</i> , lichens, mosses
pCLM ³ (peatland cushion forb, lichen and moss tundra)	<i>Saxifragaceae</i> , <i>Caryophyllaceae</i> , <i>Papaver</i> , <i>Draba</i> , lichens, mosses
WetGRS ³ (cool, flood-tolerant grass)	<i>Carex</i> spp., <i>Eriophorum</i> spp., <i>Juncus</i> spp., <i>Typha</i> spp.
pmoss ^{3,4} (peatland moss)	<i>Sphagnum</i> spp.

Table A2. Full descriptions of the PFT parameters for the four ecosystem types investigated (birch forest, tundra, peat plateau, and fen). IBS: shade-intolerant broadleaved summergreen tree; LSE: low shrubs evergreen; LSS: low shrubs summergreen; EPDS: evergreen prostrate dwarf shrubs; SPDS: summergreen prostrate dwarf shrubs; pLSE: peatland low shrubs evergreen; pLSS: peatland low shrubs summergreen; GRT: graminoid tundra; CLM: cushion forbs, lichens and mosses tundra; pCLM: peatland cushion forbs, lichens and mosses tundra; WetGRS; cool, flood-tolerant grass; pmoss: peatland moss; NL: needleleaf; BL: broadleaf; Max.: maximum; Min.: minimum; EG: evergreen; SG: summergreen; GDD5: growing degree days above 5 °C; GDD0: growing degree days above 0 °C.

Parameters	Abbreviation in LPJ-GUESS	IBS ¹	LSE _{1,2}	LSS ²	EPDS ₂	SPDS ₂	pLSE ₃	pLSS ₃	GRT ₂	CLM _{1,2}	pCLM ₃	WetGRS _{3,4}	pmoss _{3,4}
Growth form		Tree	Shrub	Shrub	Shrub	Shrub	Shrub	Shrub	Grass	Grass	Grass	Grass	moss
Leaf physiognomy		BL	NL	BL	NL	BL	NL	BL	BL	BL	BL	BL	BL
Fraction of roots in the upper/lower soil layer	rootdist	0.6/0.4	0.8/0.2	0.8/0.2	0.8/0.2	0.8/0.2	0.8/0.2	0.8/0.2	0.9/0.1	0.9/0.1	0.9/0.1	0.9/0.1	1
Max. Leaf:root C mass ratio	ltor_max	1	1	1	0.5	0.5	1	1	0.2	0.2	0.4	0.2	0.1
Min. Canopy conductance (mm/s)	gmin	0.5	0.3	0.5	0.5	0.5	0.3	0.5	0.5	0.5	0.5	0.5	0.1
Phenology types	phenology	SG	EG	SG	EG	SG	EG	SG	any	any	any	any	any
Longevity of leaves(years)	leaflong	0.3	3	0.5	3	0.5	3	0.5	0.5	0.5	0.5	0.5	1
Leaf turnover rate (year ⁻¹)	turnover_leaf	1	0.33	0.7	0.5	1	0.33	0.7	1	1	0.6	1	1
Root turnover rate (year ⁻¹)	turnover_root	0.7	0.7	0.7	0.7	0.7	0.7	0.7	0.5	0.7	0.5	0.5	0.5
Sapwood turnover rate (year ⁻¹)	turnover_sap	0.1	0.01	0.01	0.01	0.01	0.01	0.01	-	-	-	-	-
Fire resistance(0-1)	fireresist	0.1	0.12	0.12	0.12	0.12	0.12	0.12	0.5	0.5	0.5	0.5	0.5
Min. Forest floor PAR establishment (J/m ² /day)	parff_min	350000 0	10000 00	10000 00	12500 00	12500 00	10000 00	10000 00	12500 00	125000 0	125000 0	1250000	1000000
Interception coefficient	intc	0.02	0.06	0.02	0.04	0.02	0.06	0.02	0.01	0.01	0.01	0.01	0.01
Parameter for relationship between crown area and stem diameter	k_allom1	250	10	10	10	10	10	10	-	-	-	-	-
Allometry parameter related to vegetation height and stem diameter	k_allom2	60	4	4	1	1	4	4	-	-	-	-	-
Allometry parameter related to vegetation height and stem diameter	k_allom3	0.67	0.67	0.67	0.67	0.67	0.67	0.67	-	-	-	-	-
Constant in crown area and stem diameter relationship	k_rp	1.6	1.6	1.6	1.6	1.6	1.6	1.6	-	-	-	-	-
Maximum tree crown area (m2)	crownarea_max	50	1	1	1	1	1	1	-	-	-	-	-
Tree leaf to sapwood area ratio	k_latosa	6000	125	125	100	100	125	125	-	-	-	-	-

Sapwood and heartwood density (kgC/m3)	wooddens	200	250	250	200	200	250	250	-	-	-	-	-
Growth efficiency threshold (kgC/m2leaf/yr)	greff_min	0.04	0.012	0.012	0.01	0.01	0.012	0.012	-	-	-	-	-
Max. Establishment rate (samplings/m2/yr)	est_max	0.2	0.75	0.8	0.8	0.8	0.35	0.8	-	-	-	-	-
Recruitment shape parameter	alphar	10	10	10	10	10	10	10	-	-	-	-	-
Mean non_stress longevity	longevity	300	25	25	30	30	25	25	-	-	-	-	-
GDD5 ramp for phenology	phengdd5ramp	190	0	50	0	50	0	50	50	1	1	100	75
Photosynthesis min temperature (°C)	pstemp_min	-4	-4	-4	-4	-4	-4	-4	-4	-4	-4	-5	-4
Approximate lower range of temperature optimum for photosynthesis	pstemp_low	10	10	10	10	10	10	10	10	10	10	5	10
Aproximate upper range of temperature optimum for photosynthesis	pstemp_high	25	25	25	20	20	25	25	25	25	25	30	30
Photosynthesis max temperature (°C)	pstemp_max	38	38	38	38	38	38	38	38	38	38	45	38
Min. Temperature of coldest month for survival	tmin_surv	-30	-32.5	-40	-1000	-1000	-32.5	-40	-1000	-1000	-1000	-1000	-1000
Min. Temperature of coldest month for establishment	tmin_est	-30	-32.5	-40	-1000	-1000	-32.5	-40	-1000	-1000	5	-1000	-1000
Max. Temperature of coldest month for establishment	tmax_est	3	1000	1000	1000	1000	1000	1000	1000	1000	1000	1000	15.5
Min. Temperature of warmest month for establishment	twmin_est	-1000	-1000	-1000	-1000	-1000	-1000	-1000	-1000	-1000	-1000	-1000	-1000
Min. GDD5 for establishment	gdd5min_est	350	100	100	0	0	75	100	100	0	0	0	0
Min. GDD0 for reproduction	zero_min	500	300	300	150	150	300	300	500	50	50	150	0
Max. GDD0 for reproduction	zero_max	-	-	-	1500	350	-	-	1000	150	150	150	5000
Min. Snow cover (mm)	min_snow	-	-	-	20	20	-	-	-	50	50	-	-
Maintenance respiration coefficient	respcoeff	1	1	1	1	1	1	1	1	1	1	1	2
Min. fraction of available soil water in upper soil layer in the growing season	drought_tolerance	0.46	0.1	0.1	0.01	0.01	0.1	0.1	0.01	0.01	0.01	0.01	1
Maximum water table position for establishment (mm)	wtp_max	-301	-301	-301	-301	-301	-250	-250			-200	100	0
Max. inundation duration (days) before GPP is reduced to 0	inund_duration	-	-	-	-	-	5	5	-	-	31	31	15
Max. evapotranspiration rate	emax	5	5	5	5	5	5	5	5	5	5	5	1
Litter moisture flammability threshold (fraction of AWC)	litterme	0.3	0.3	0.3	0.3	0.3	0.3	0.3	0.2		0.2	0.2	0.2

Sapwood C:N mass ratio	cton_sap	330	330	330	300	300	330	330	-	-	-	-	-
Fine root C:N mass ratio	cton_root	29	29	29	29	29	29	29	29	29	29	29	50
Maximum nitrogen uptake per fine root [kgN kgC-1 day-1]	nuptoroot	0.003	0.0028	0.0028	1	1	0.0028	0.0028	1	1	0.00551	0.00551	0.00551
Half-saturation concentration for N_uptake [kgN L-1]	km_volume	1.5E-06	1.5E-06	1.5E-06	1.5E-06	1.5E-06	1.5E-06	1.5E-06	1.9E-06	1.9E-06	1.9E-06	1.9E-06	1.9E-06
Fraction of sapwood or root (for herbaceous PFTs) for N longterm storage	fnstorage	0.15	0.3	0.3	0.3	0.3	0.3	0.3	0.3	0.3	0.3	0.3	0.3
Isoprene emission capacity (ug C g-1 h-1)	eps_iso (Is30/Is20)*	45	1.737	6.85	1.4	14.003	1.737	2	9.818	1.198	1.29	1.198	1.2
Isoprene emissions show a seasonality (1) or not(0)	seas_iso	1	0	1	0	1	0	1	1	0	0	0	0
Monoterpene emission capacity (ug C g-1 h-1)	eps_mon (Ms30/Ms20)*	0.52/0.08	0.088	0.748	1.301	0.425	0.088	0.748	0	0	0	0	0
Fraction of monoterpene production that goes into storage pool	storfrac_mon	0.4	0.5	0.5	0.5	0.5	0.5	0.5	0.5	0	0	0	0
Aerodynamic conductance (m s-1)	ga	0.04	0.04	0.04	0.03	0.03	0.04	0.04	0.03	0.03	0.03	0.03	0.03

1 Denotes PFT's belonging to the birch forest site. 2 Denotes PFT's belonging to the tundra site. 3 Denotes PFT's belonging to the peat plateau site. 4 Denotes PFT's belonging to the fen site.

B. Extended description of the input data

Four gaps in daily radiation data from ANS (1 January–30 June 1984, 9–16 June 2016, 13–15 February 2007, 23 July–17 August 2011) were filled with the Princeton reanalysis dataset (Sheffield et al., 2006) for the grid cell nearest Abisko. Given their vicinity and similar elevation (altitudinal range <100 m), the birch forest, peat plateau, and tundra sites were run with climate data from the ANS data set (1913–2018; ANS 2020), whereas the fen site used data from Katterjokk Station (1973–2018; SMHI) and bias-corrected daily data (1913–1972) from the ANS.

C. Full details of the WWE manipulation experiments

We selected six CMIP6 climate scenarios from two general circulation models (GCMs) with different climate sensitivities, i.e., CanESM5 and GFDL-ESM4, and three shared socioeconomic pathways representing three levels of varying greenhouse gas projections, i.e., SSP119, SSP270, and SSP585. The SSPs are narratives describing how global society, demographics, and economics could change over this century, and whether and how different radiative forcing levels (Representative Concentration Pathways, or RCPs) can be reached under these narratives (Riahi et al., 2017). The resulting scenario names are a combination of the SSP narratives and the RCP radiative forcings, and include a broad range of scenarios in which mitigation and adaptation challenges vary from low to very high (SSP119: SSP1 and SSP585: SSP5, with the radiative forcing reaching 1.9 and 8.5 W m² respectively at the end of this century).

For each scenario (n=6), daily meteorological data (1950-2100) for the gridcell near the Torneträsk area was extracted, and then bias-corrected at daily scale against the observed meteorological data using the period 1985-2014, based on the method described in Hawkins et al., (2013). Since GCMs tend to overestimate the number of low-magnitude rain events as compared to observations (Gutowski et al., 2003), precipitation events below a certain threshold (1.5 mm and 1 mm for the ANS and Katterjokk Station data, respectively) were removed in the GCM's output before bias-correction to realistically match the observed wet-day frequency at each site.

Table C1. The four WWE indices used to create the WWE manipulation experiments S1, S2, and S3. The indices were computed using mean daily air temperature (T) and daily precipitation sum (P). Adapted from Vikhamar-Schuler et al. (2016).

Index Number	Name	Description
1	Frequency of melt days	$T > 0^{\circ}\text{C}$
2	Intensity of melt days	$\sum_{days=1}^n (T > 0^{\circ}\text{C})$
3	Frequency of ROS	$T > 0^{\circ}\text{C}$, and $P > 1 \text{ mm}$
4	Intensity of ROS	$\sum_{days=1}^n (T > 0^{\circ}\text{C}, \text{ and } P > 1 \text{ mm})$

Table C2. Full details of the monthly anomalies in each of the four WWE indices and each of the six CMIP6 scenarios from the Abisko Station and Katterjokk Station datasets, calculated for November to March based on the periods of 2071-2100 and 1985-2014.

		WWE anomalies for the Abisko dataset					WWE anomalies for the Katterjokk dataset				
WWE index	CMIP6 scenario	January	February	March	November	December	January	February	March	November	December
Index 1. Melt days	CanESM5 SSP119	2	2	1	8	5	2	2	0	8	4
	CanESM5 SSP270	6	3	7	15	13	6	2	4	14	12
	CanESM5 SSP585	11	8	12	20	20	11	7	9	21	19
	GFDL-ESM4 SSP119	1	0	0	2	0	1	0	-1	1	0
	GFDL-ESM4 SSP270	2	1	1	4	2	2	1	1	4	2
	GFDL-ESM4 SSP585	6	2	4	11	5	6	2	4	10	5
Index 2. Positive degree days (°C)	CanESM5 SSP119	1.9	2.6	1.3	32.7	12.2	1.7	2.0	0.7	26.7	9.5
	CanESM5 SSP270	11.3	3.3	9.4	57.0	34.0	10.7	2.5	4.8	45.5	26.7
	CanESM5 SSP585	25.2	12.1	24.7	119.3	80.2	24.0	9.6	15.2	103.2	68.9
	GFDL-ESM4 SSP119	0.7	0.6	-1.3	4.2	-0.4	0.7	0.5	-0.8	3.2	-0.6
	GFDL-ESM4 SSP270	2.6	1.0	2.1	15.6	3.9	2.4	0.8	1.3	12.5	2.7
	GFDL-ESM4 SSP585	12.5	3.1	9.8	40.3	10.6	11.9	2.4	6.3	32.0	7.8
Index 3. Melt and precipitation days	CanESM5 SSP119	1	1	0	3	2	1	1	0	5	3
	CanESM5 SSP270	3	1	3	5	5	4	1	2	8	6
	CanESM5 SSP585	5	3	4	7	7	7	4	5	11	10
	GFDL-ESM4 SSP119	1	0	-1	1	0	1	0	-1	1	1
	GFDL-ESM4 SSP270	1	1	0	2	1	1	1	0	3	2
	GFDL-ESM4 SSP585	4	1	2	5	3	5	1	3	7	3
Index 4. Cumulative rain during Index 3 (mm)	CanESM5 SSP119	2.9	3.4	0.9	10.1	2.6	8.8	9.7	1.3	36.8	10.3
	CanESM5 SSP270	8.2	3.1	6.5	12.8	11.8	24.8	8.1	15.1	47.1	37.0
	CanESM5 SSP585	12.8	9.8	10.2	19.7	22.1	40.1	28.2	31.3	72.8	70.7
	GFDL-ESM4 SSP119	4.1	0.5	-2.3	1.5	1.9	10.9	1.9	-4.5	4.2	5.6
	GFDL-ESM4 SSP270	3.5	2.6	-0.2	6.2	3.6	9.1	7.4	1.9	19.9	12.0
	GFDL-ESM4 SSP585	9.9	2.5	4.0	10.1	6.5	28.9	8.5	15.7	36.3	20.8

Table C3. In the top panel are displayed the monthly anomalies in air temperature (in °C) and precipitation (%) in each of the six CMIP6 scenarios from the Abisko Station and Katterjokk Station datasets, calculated for November to March based on the periods of 2071-2100 and 1985-2014.

Climate variable	CMIP6 scenario	Climate anomalies from the Abisko dataset					Climate anomalies from the Katterjokk dataset				
		January	February	March	November	December	January	February	March	November	December
Air temperature	CanESM5 SSP119	2.6	3.3	1.5	4.1	3.2	2.6	3.3	1.5	4.1	3.2
	CanESM5 SSP270	5.8	5.3	4.3	6.1	7.0	5.8	5.3	4.3	6.1	7.0
	CanESM5 SSP585	8.5	8.2	6.2	8.7	9.7	8.5	8.2	6.2	8.7	9.7
	GFDL-ESM4 SSP119	1.2	1.7	0.8	1.3	-0.1	1.2	1.7	0.8	1.3	-0.1
	GFDL-ESM4 SSP270	2.8	2.5	2.0	2.5	2.5	2.8	2.5	2.0	2.5	2.5
	GFDL-ESM4 SSP585	5.7	4.3	3.7	4.9	4.3	5.7	4.3	3.7	4.9	4.3
Precipitation	CanESM5 SSP119	-22.4	0.6	12.1	-25.2	17.6	22.4	0.6	12.1	-25.2	17.6
	CanESM5 SSP270	-16.5	14.1	-10.8	-31.3	-8.3	16.5	14.1	-10.8	-31.3	-8.3
	CanESM5 SSP585	4.2	-10.3	-32.3	-48.9	-34.1	-4.2	-10.3	-32.3	-48.9	-34.1
	GFDL-ESM4 SSP119	27.6	-9.2	8.0	-16.1	-9.5	-27.6	-9.2	8.0	-16.1	-9.5
	GFDL-ESM4 SSP270	-2.4	-12.7	12.1	-19.7	-2.9	2.4	-12.7	12.1	-19.7	-2.9
	GFDL-ESM4 SSP585	8.5	11.3	-4.0	-20.1	-7.0	-8.5	11.3	-4.0	-20.1	-7.0

D. Sensitivity analysis

Methodology

Snow properties and processes were first calibrated before evaluating the modelled seasonal dynamics and responses to WWE of snowpack and soil temperature at each site. Hence, site level sensitivity analysis (SA) were conducted to explore the contribution of different parameters and parameter interactions to the estimated snow density, snow depth, snow temperature, and soil temperature during the autumn (October-December) and winter (January-April) seasons, and during specific WWE at each site (except for the tundra site due to lack of observational data for calibration and evaluation). The contribution of the selected parameters was quantified using the variance-based Sobol sensitivity index (Saltelli, 2002; Saltelli and Annoni, 2010). Sobol sensitivity analysis assumes that the model output variations can be decomposed into different subcomponents (Pappas et al., 2008). The main contribution of each parameter to the output variance is quantified by a first-order index, while the overall parameter contribution is quantified by the total-order index, which includes the parameter's interactions with other parameters. In this study, each parameter was sampled 1000 times using the pseudo-random Sobol sequence, while cross-sampling between parameters was done based on the Saltelli method (Saltelli et al. 2008). A plausible range for each parameter was defined based on our current knowledge, literature survey or assigning a certain percentage of changes. The tested parameters and parameter ranges are presented in Table D1. In total, we tested 18.000 simulations for every site (8 parameters) except the "tundra" site due to the limited observational data available. The first-order and total-order Sobol indices for the autumn and winter seasons were calculated based on each simulation's seasonal output average for the period 2001-2010 in the birch forest and fen sites, and for the period 2006-2012 in the peat plateau site. For each site, we compared the modelled snow depth and GT of the 18.000 simulations with observational data from 2001-2010 (2006-2012 in the peat plateau), and selected the parameter values that better depicted each site's seasonal conditions.

In addition, a pre-evaluation of the modelled CO₂ fluxes with the observations using the default quantum efficiency (the rate at which plants convert light into chemical energy; α_{c3}) value (0.08) indicated a large overestimation of both GPP and ER in the tundra site. Hence, we used an α_{c3} value of 0.07 for the tundra PFTs which resulted in more accurately modelled CO₂ fluxes than the default value of 0.08 (Tang et al. 2016).

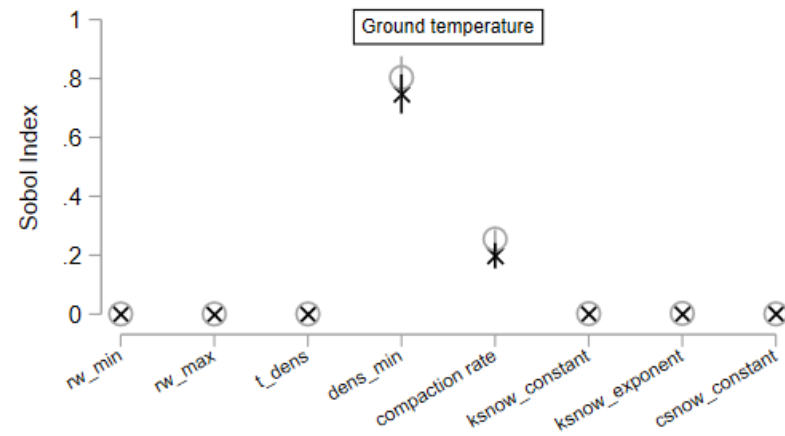
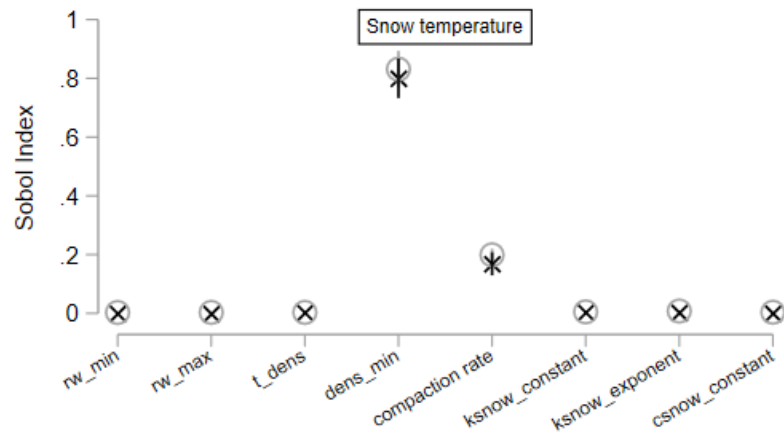
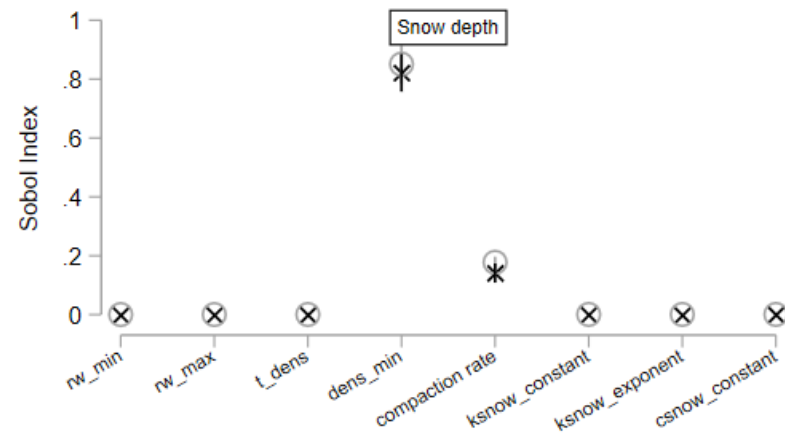
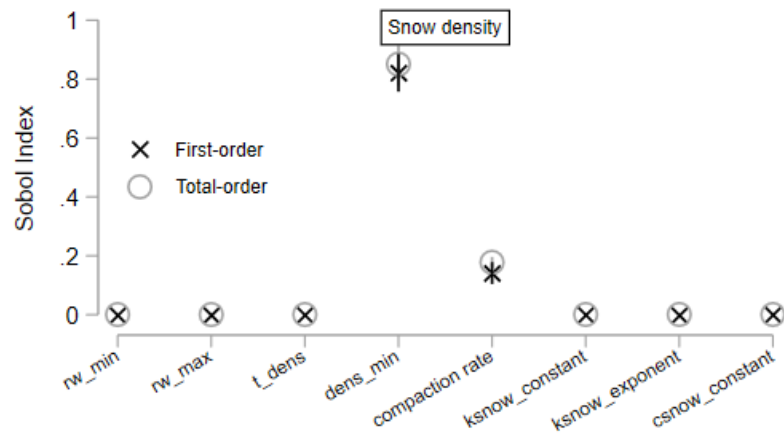
Table D1. Detailed description of the 8 parameters investigated in the SA, the process in which they are involved, their standard values, and their uncertainty ranges based on the literature or on certain percentage of changes from the original values.

Parameter	Minimum	Maximum	Standard Values	Units	Description
rw_min	0.02	0.06	0.03	Fraction	Minimum fraction of water that can be hold in the snowpack (Anderson et al., 1976)
rw_max	0.1	0.15	0.1	Fraction	Maximum fraction of water that can be hold in the snowpack (Singh et al., 1997)
dens_t	300	550	400	Kg m-3	Maximum density of snow (D'Amboise et al., 2017)
dens_min	50	200	150	Kg m-3	Minimum density of fresh snow (Vionnet et al., 2012)
compaction_rate	0.5	1.5	1	-	Scale factor by which snow compaction is multiplied to either slow down or accelerate the compaction of snow.
ksnow_constant	2	2.44	2.22	-	Empirical constant used to calculate the snow thermal conductivity. Range modified from that of Best et al. (2011) to increase or decrease the snow thermal conductivity up to c. 10%
cnow_constant	0.61	0.77	0.689	-	Empirical constant used to calculate the snow heat capacity. Range modified from that of Fukusako et al. (1990) to increase or decrease the snow heat capacity up to c. 10%
ksnow_constant	1.8	2	1.88	-	Empirical constant used to calculate the snow thermal conductivity. Range modified from that of Best et al. (2011) to increase or decrease the snow thermal conductivity up to $\geq 10\%$

Results

a) Sobol indices for seasonal output

a) BIRCH FOREST – Autumn 2001 - 2010



b)

BIRCH FOREST – Winter 2001 - 2010

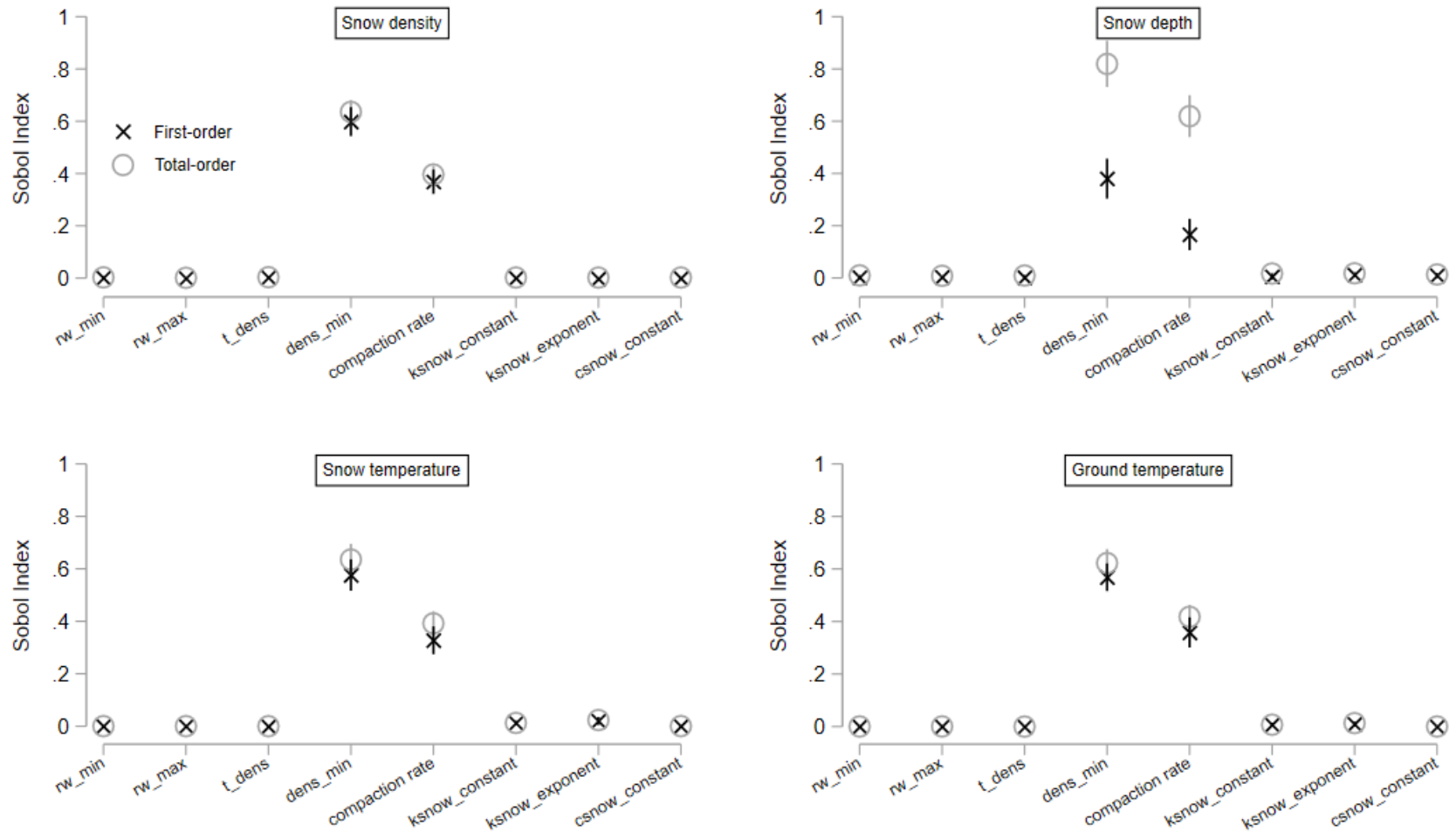
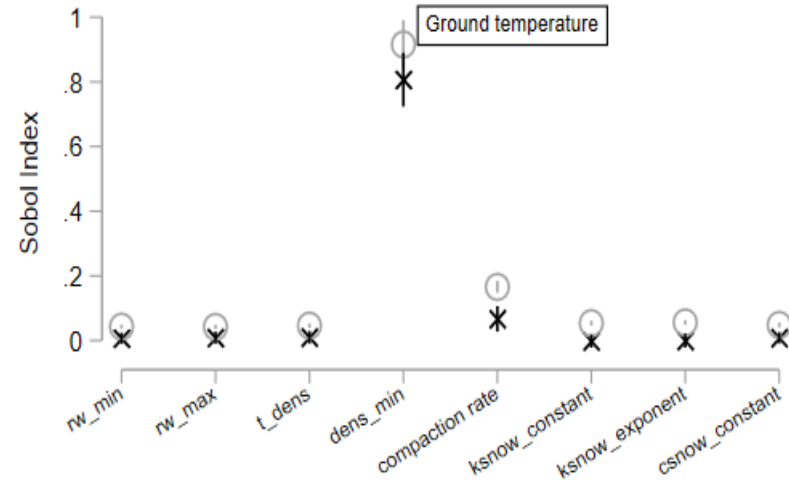
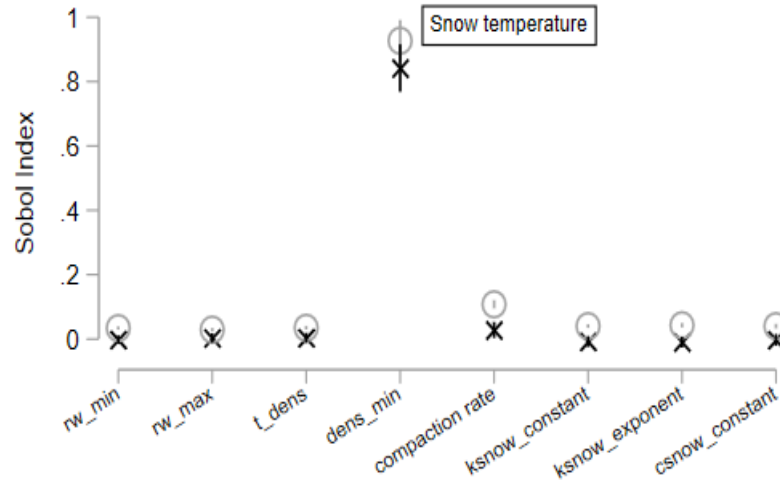
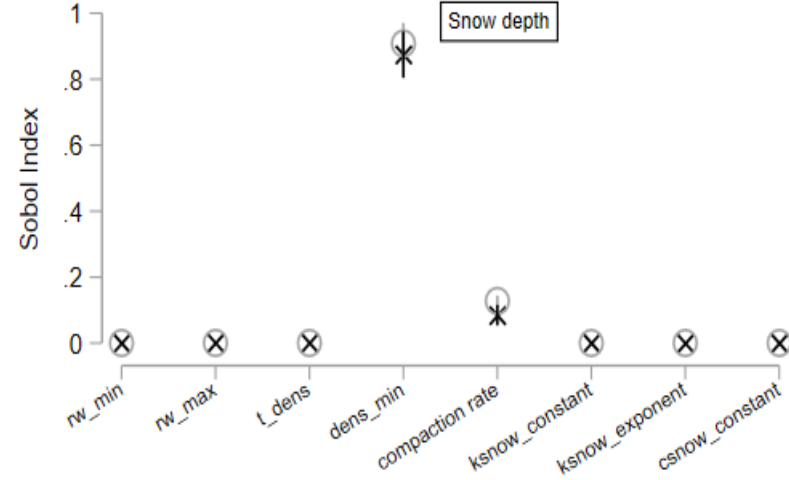
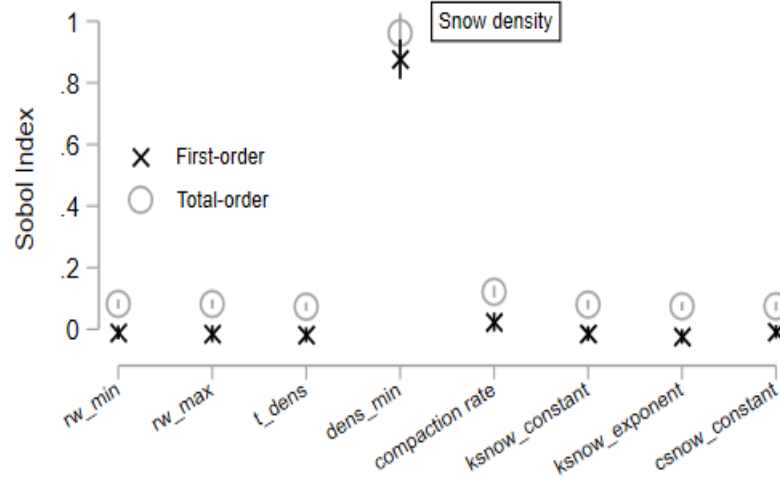


Figure D1. First- and total-order Sobol indices of the eight examined parameters for snow depth, snow density, snow temperature, and ground temperature, at the birch forest, during the autumn (a) and winter seasons (b) in 2001-2010.

a)

PEAT PLATEAU – Autumn 2006 – 2012



b)

PEAT PLATEAU – Winter 2006 – 2012

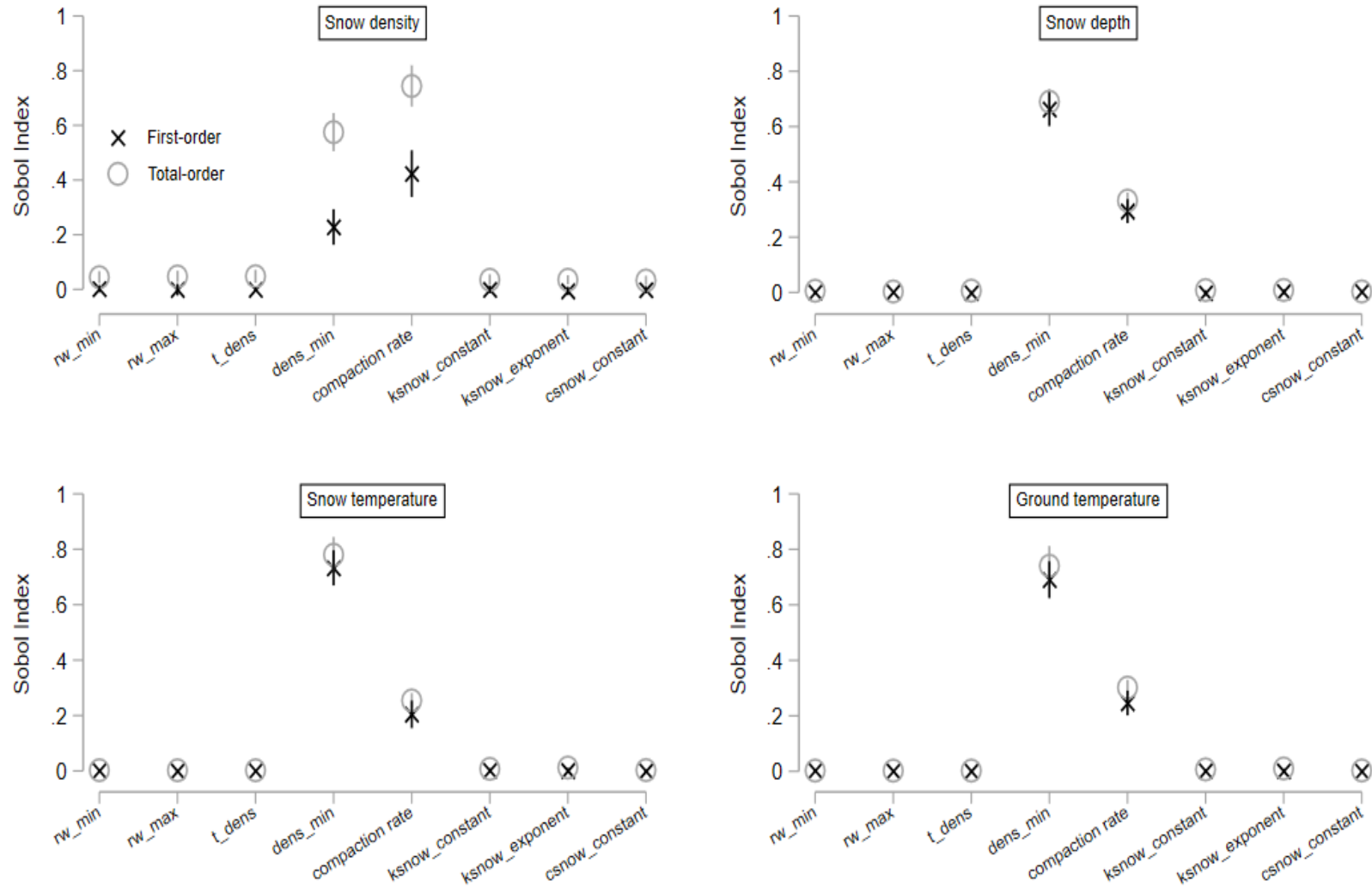
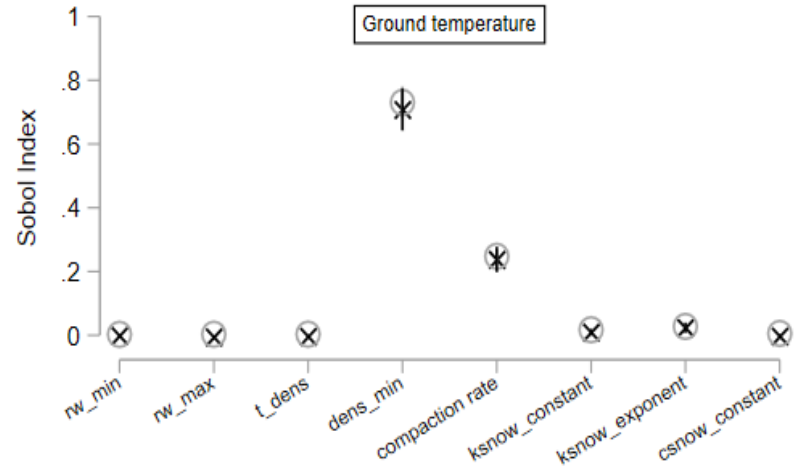
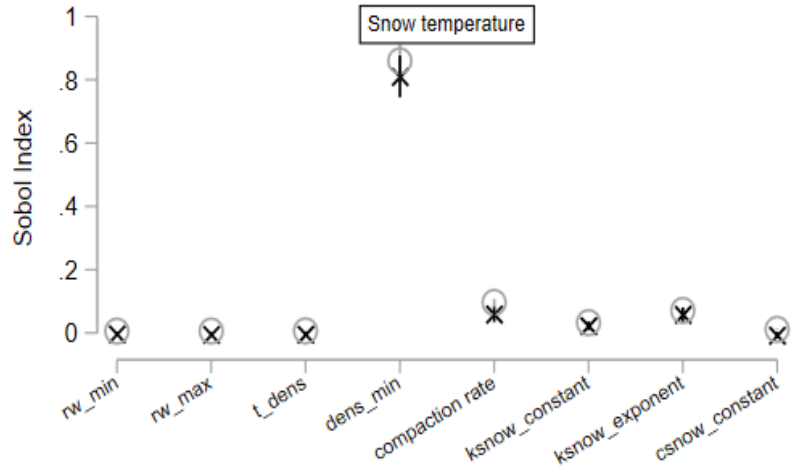
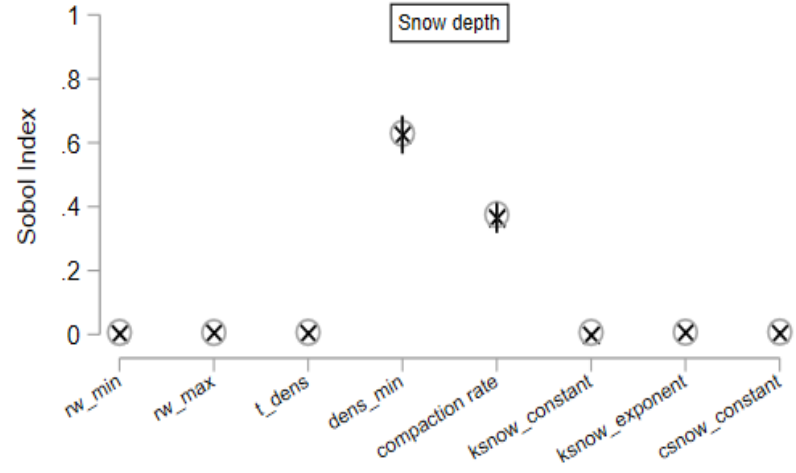
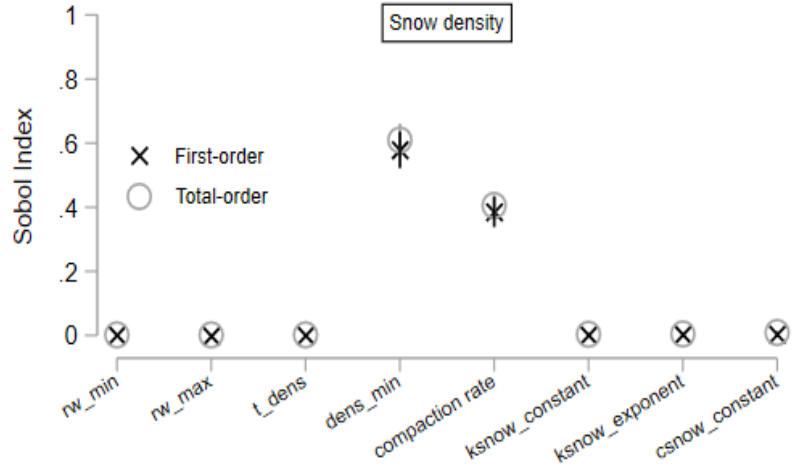


Figure D2. First- and total-order Sobol indices of the eight examined parameters for snow depth, snow density, snow temperature, and ground temperature, at the peat plateau, during the autumn (a) and winter seasons (b) in 2006-2012.

a)

FEN – Winter 2001 - 2010



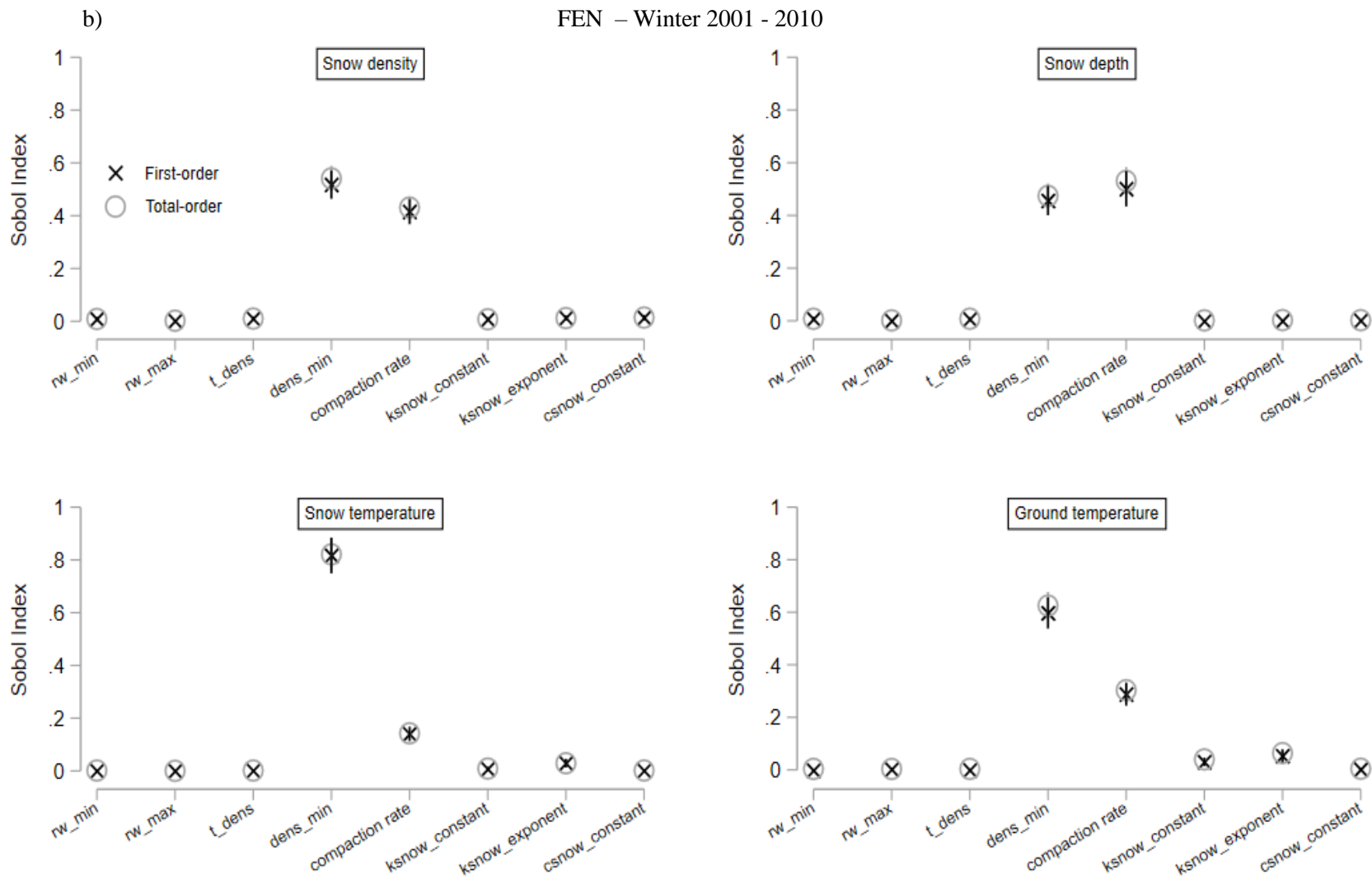


Figure D3. First- and total-order Sobol indices of the eight examined parameters for snow depth, snow density, snow temperature, and ground temperature, at the fen, during the autumn (a) and winter seasons (b) in 2001-2010.

b) Comparing measured vs modelled seasonal values

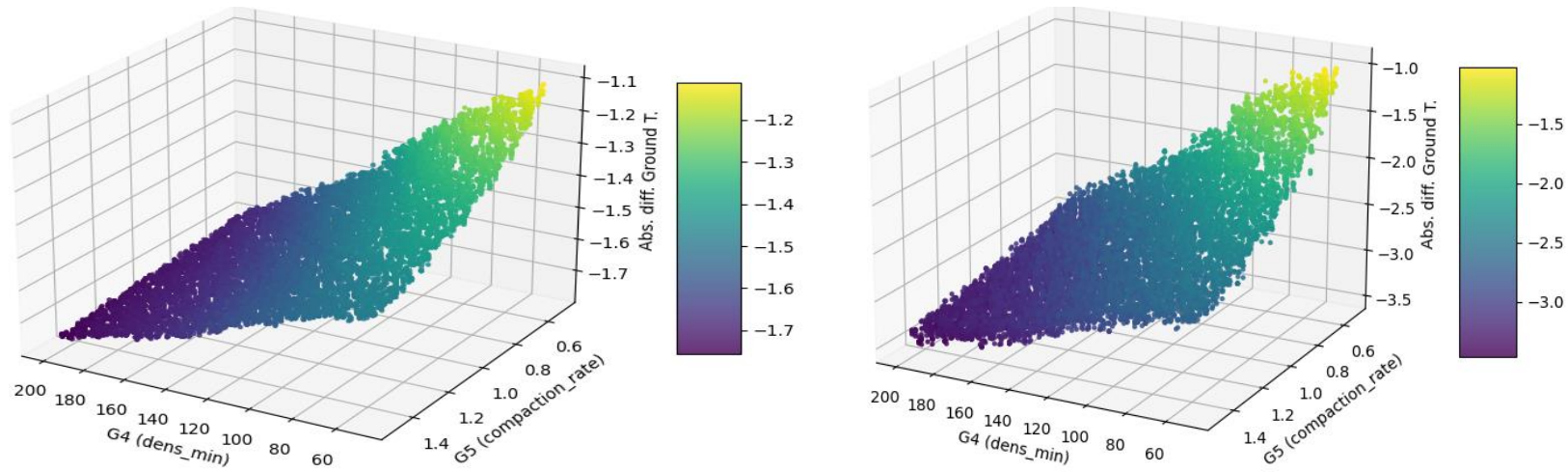


Figure D4. The absolute modelled vs observed difference in ground temperature at the birch forest site, during the autumn (left) and winter (right) seasons in 2001-2010.

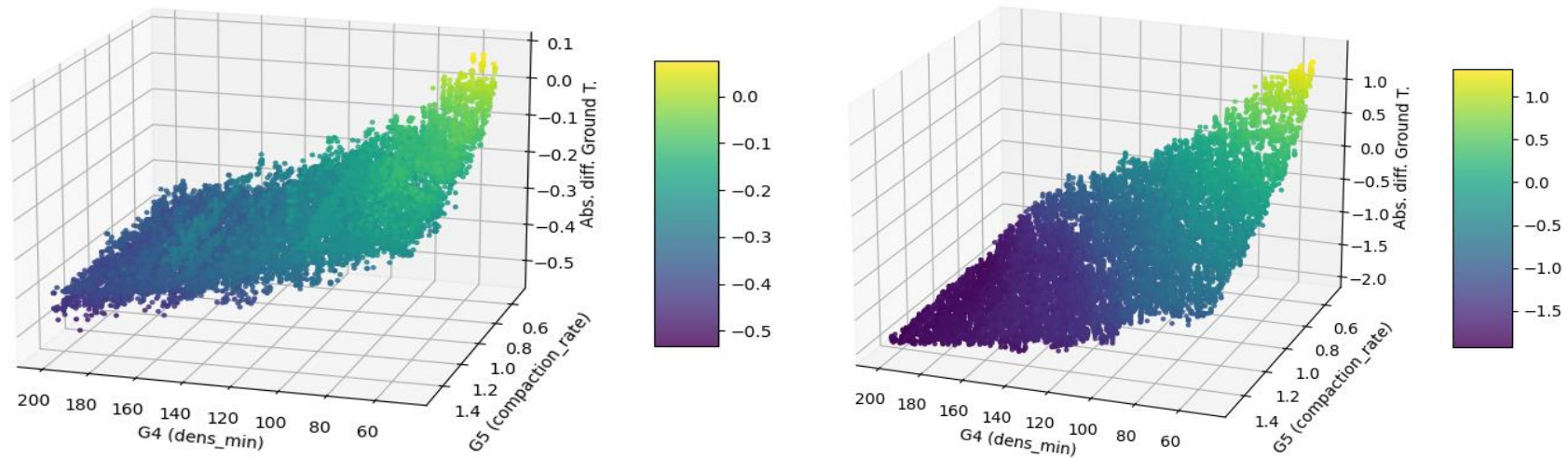


Figure D5. The absolute modelled vs observed difference in ground temperature at the peat plateau site, during the autumn (left) and winter (right) seasons in 2006-2012.

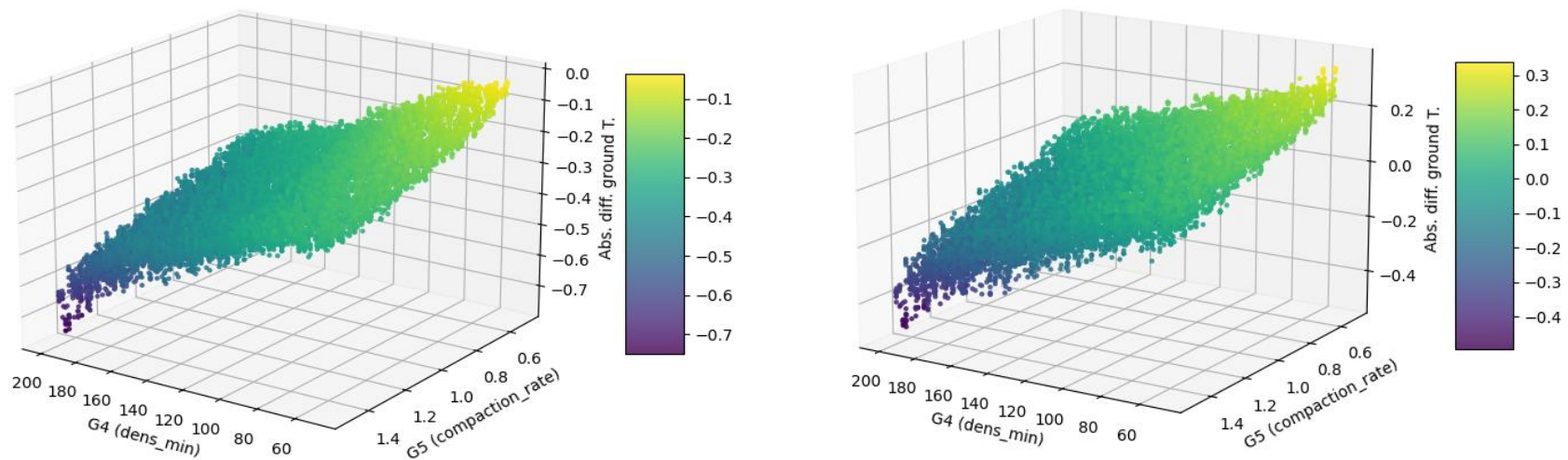


Figure D6. The absolute modelled vs observed difference in ground temperature at the fen site, during the autumn (left) and winter (right) seasons in 2001-2010.

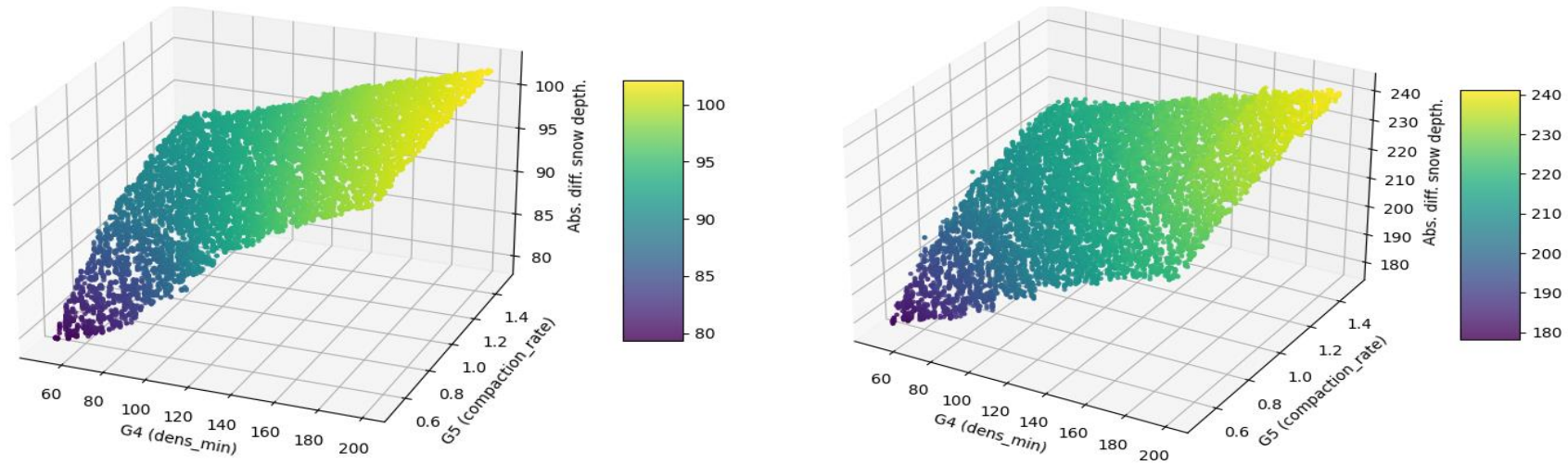


Figure D7. The absolute modelled vs observed difference in snow depth at the birch forest site, during the autumn (left) and winter (right) seasons in 2001-2010.

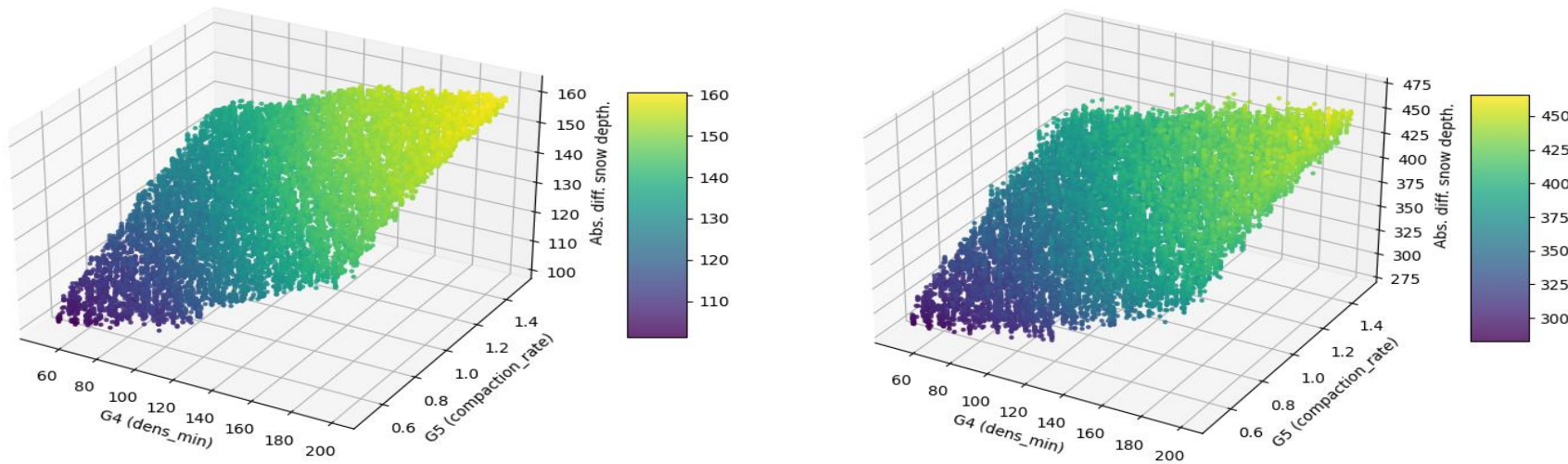


Figure D8. The absolute modelled vs observed difference in snow depth at the fen site, during the autumn (left) and winter (right) seasons in 2001-2010.

E. Model evaluation

Table E1. Full details of the observation data from the Torneträsk area used to evaluate model's performance.

Data	Time period	Site	Reference
Snow depth	2011 - 2018	Birch forest, peat plateau, fen	ANS 2020
Ground temperature	2011 - 2018	Birch forest	ANS 2020
Ground temperature	Growing-season 2011	Tundra	A. Michelsen, not published
Ground temperature	2013 - 2018	Peat plateau	M. Johansson, not published
Ground temperature	2019- 2020	Fen	D. Pascual, not published
Eddy Covariance NEE	2007- 2009	Birch forest	(Heliasz, 2012)
Ec-tower measured NEE	2016 - 2018	Peat plateau (from Stordalen)	ICOS 2019
Eddy Covariance NEE	2006 - 2008	Fen (from Stordalen)	(Christensen et al., 2012)
Chamber-measured NEE	Growing season 2010-2012	Tundra	(Finderup Nielsen et al. 2019)
Chamber-measured GPP	Growing season 2010-2012	Tundra	(Finderup Nielsen et al. 2019)
Chamber-measured Reco	Growing season 2010-2012	Tundra	(Finderup Nielsen et al. 2019)
EC-tower measured CH ₄	2016 - 2017	Peat plateau (from Stordalen)	ICOS 2019
EC-tower measured CH ₄	2006 to 2007	Fen (from Stordalen)	(Jackowicz-Korczynski et al., 2010)

Evaluation of physical and biogeochemical variables in the historical period

Evaluation of physical variables

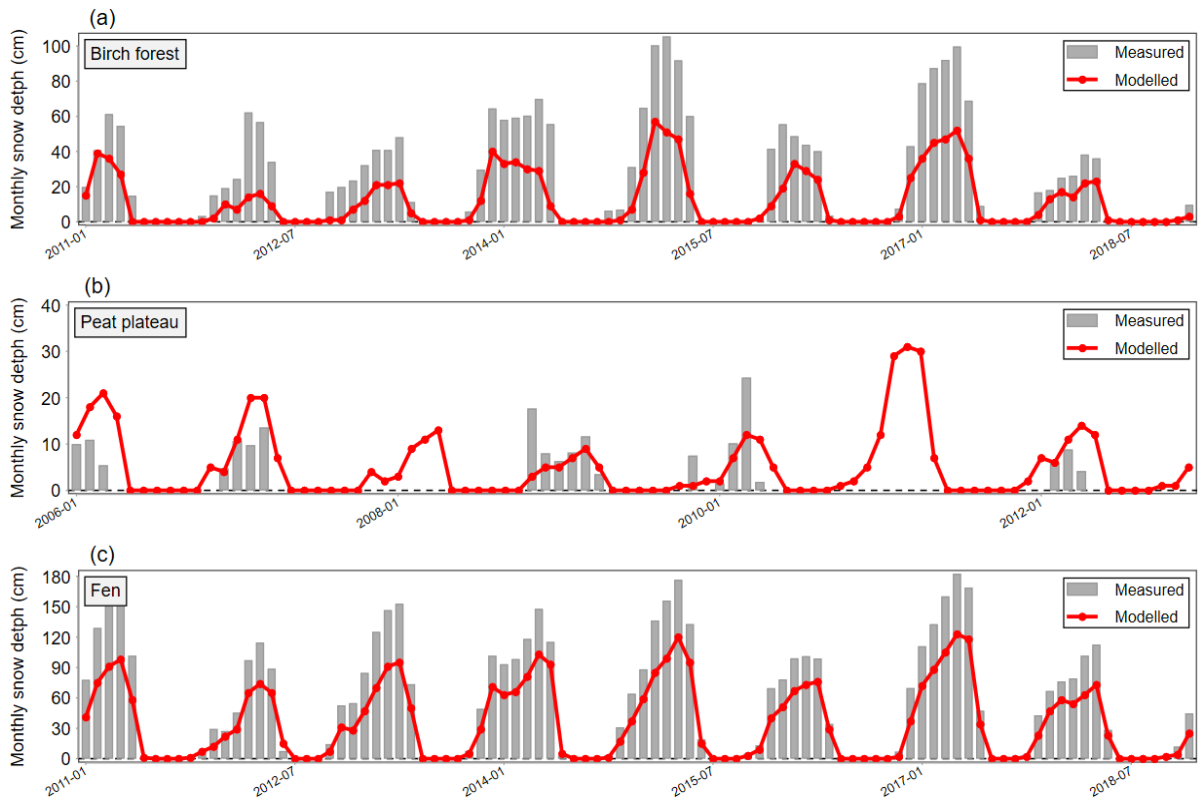


Figure E1. Modeled and measured monthly snow depth at the birch forest (a), peat plateau (b), and fen sites (c). At the peat plateau, the measured data is very scarce and monthly means are based on very few or even single measurements.

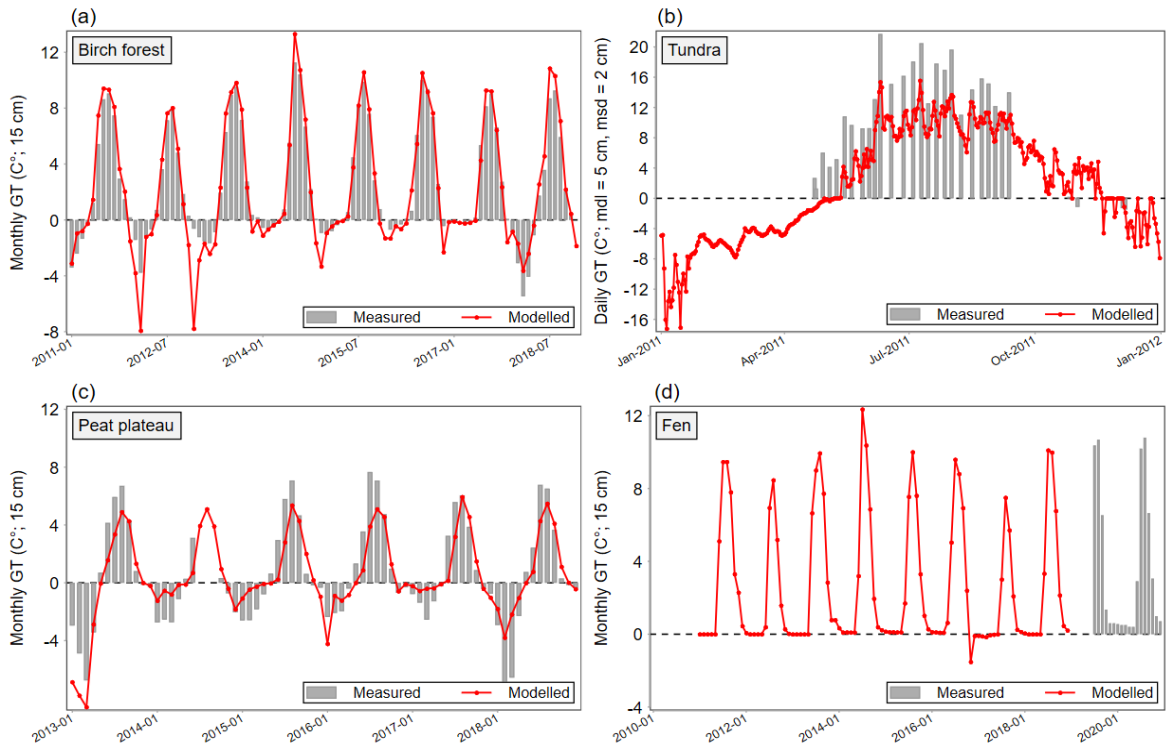


Figure E2. Modeled and measured monthly ground temperatures (GT) at the birch forest (a), peat plateau (c), and fen sites (d), and daily GT in the growing season at the tundra site (b).

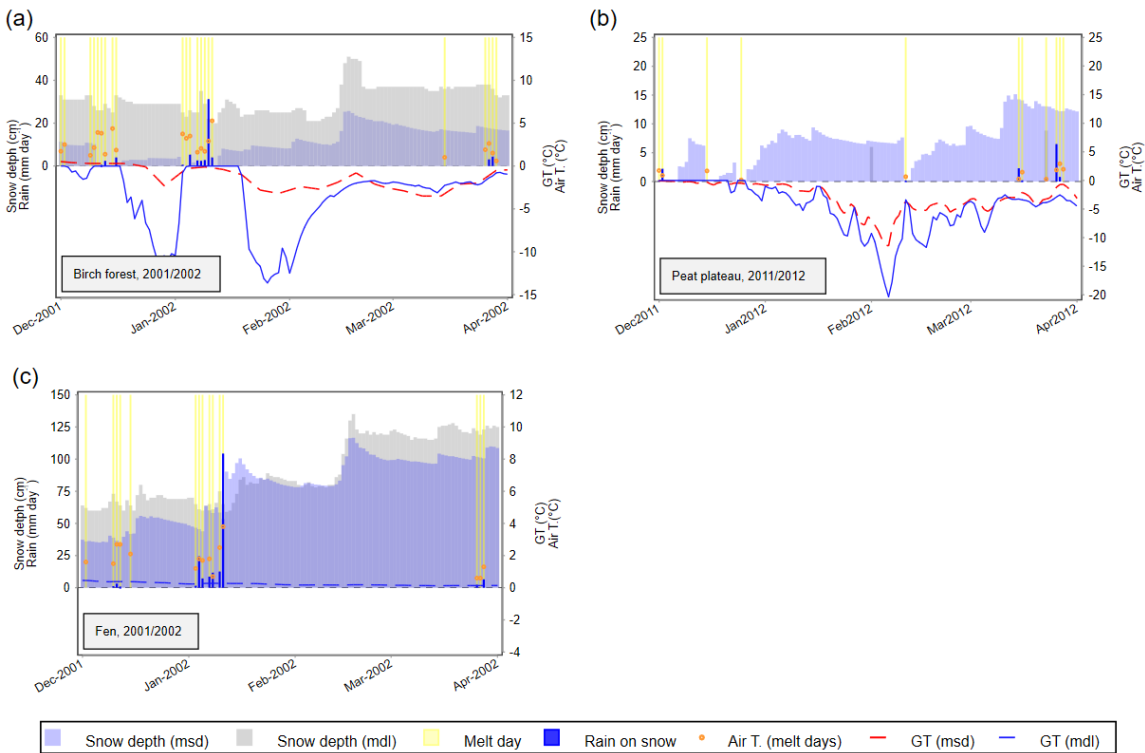


Figure E3. Modelled and measured snow depth and ground temperature from December to March in two of the years with the highest frequencies and intensities of WWE measured in the study area (2002 and 2012; Pascual & Johansson, 2022). Yellow bars and orange dots denote melt days and their measured mean daily air temperature, respectively. Blue bars indicate the occurrence of liquid precipitation (rain) and the measured amounts in mm.

Evaluation of biogeochemical variables

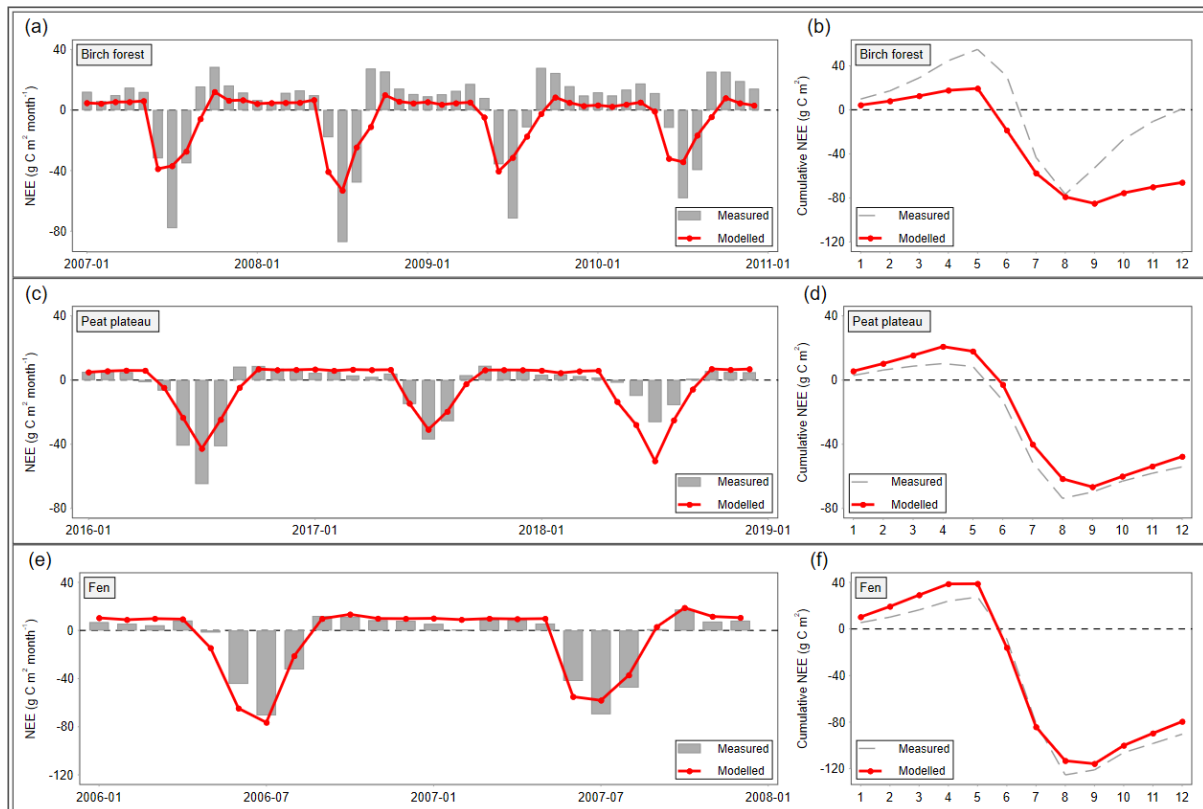


Figure E4. Modelled and measured monthly (left) and mean annual cumulative (right) CO₂ net ecosystem exchange (NEE) fluxes for the birch forest (a-b), tundra (c-d), and peat plateau (e-f) sites. Positive values indicate ecosystem release to the atmosphere and negative values indicate ecosystem uptake.

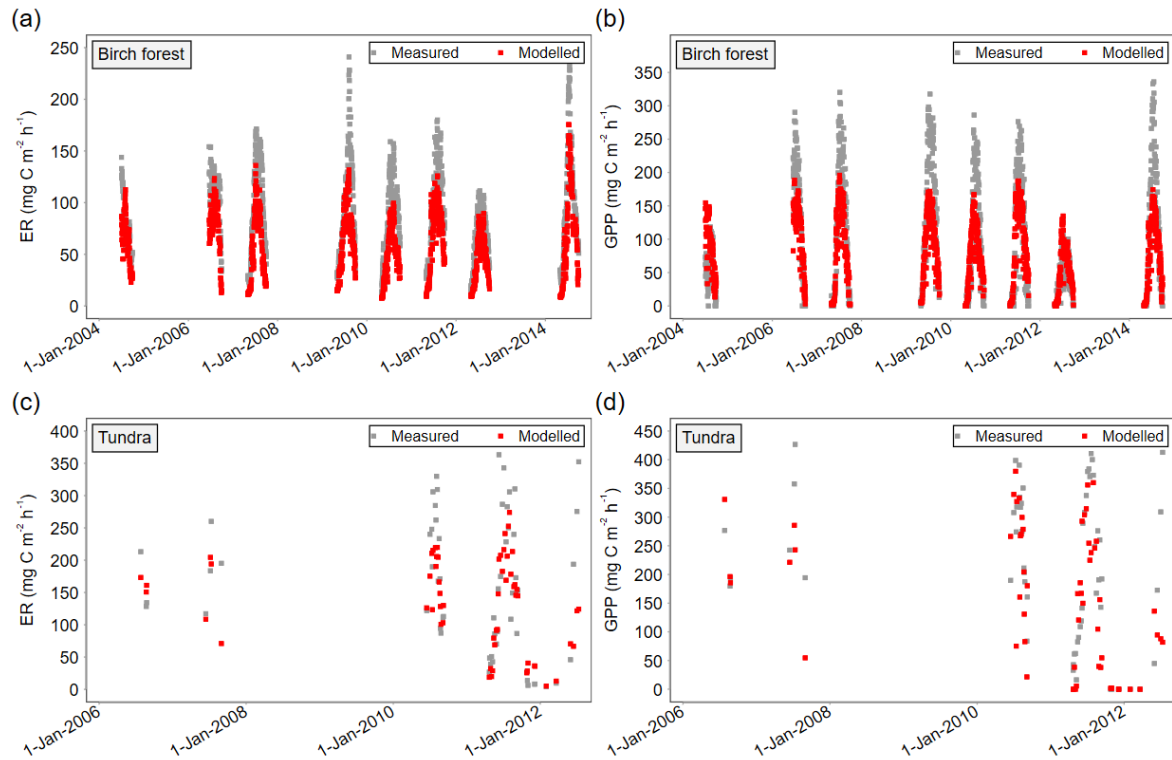


Figure E5. Modeled and measured daily ecosystem respiration (ER; left column) and gross primary production (GPP; right column) in the growing-season at the birch forest (a-b) and tundra (c-d) sites.

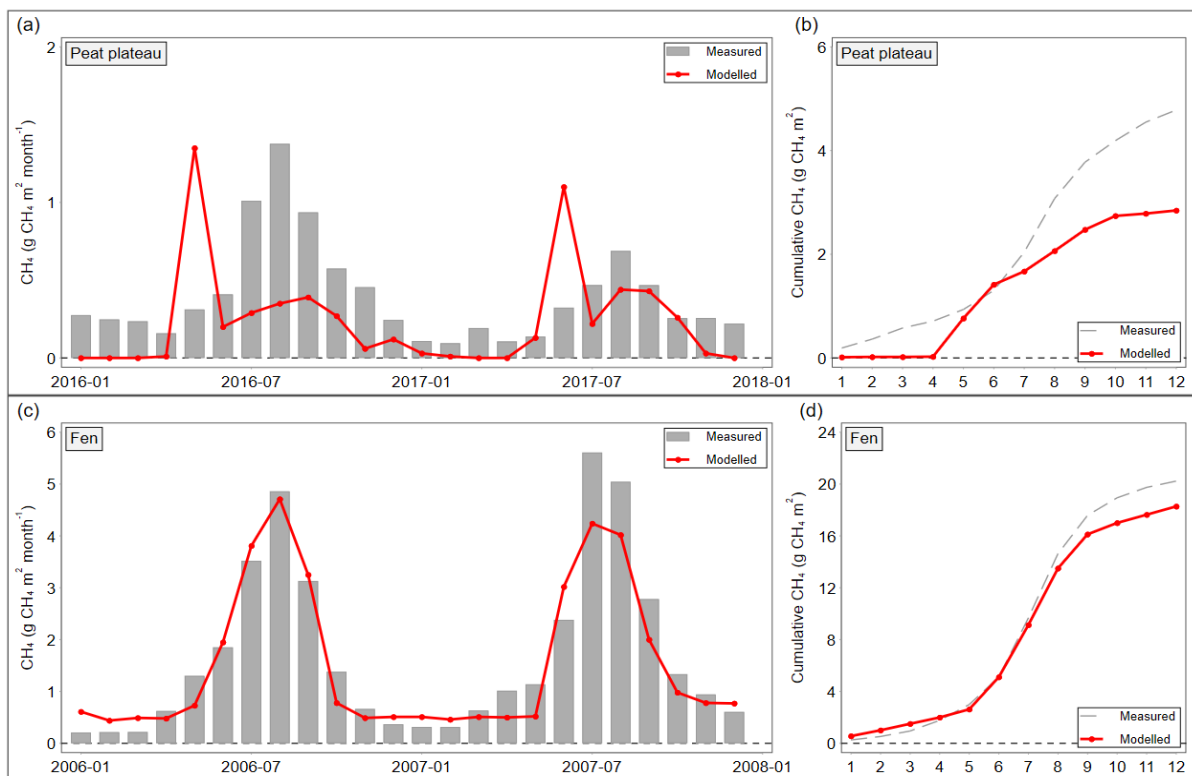


Figure E6. Modelled and measured monthly (left) and mean annual cumulative (right) CH₄ fluxes for the peat plateau (a-b) and fen (c-d) sites.

F. Impacts of WWE on physical variables

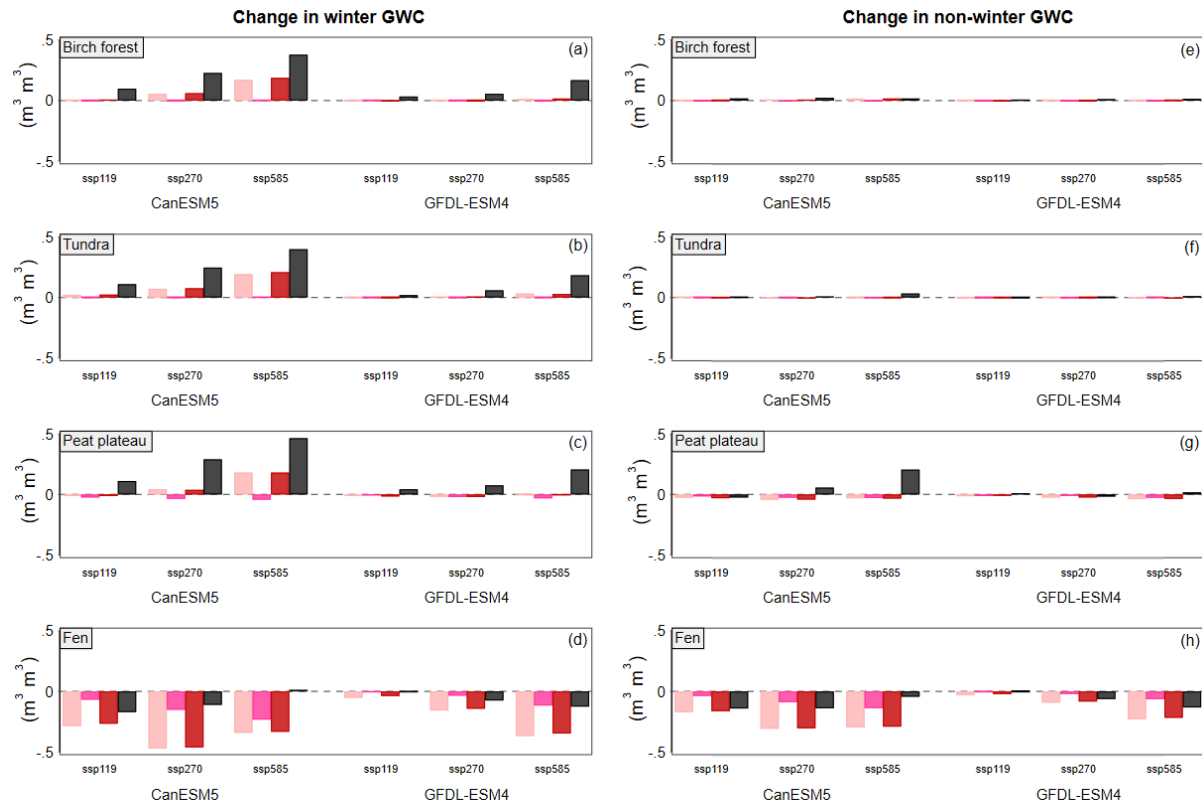


Figure F1. Differences between the model output of the MANIPULATION runs (S1, light pink; S2, pink; S3, red; S4, dark grey) and the HISTORICAL runs (S0), for the variables winter GWC ($\text{m}^3 \text{m}^{-3}$; left column), and non-winter GWC ($\text{m}^3 \text{m}^{-3}$; right column), at each of the simulated sites. Differences calculated by subtracting each of the MANIPULATION (S1-S4) from the FORCING (S0) simulation outputs.

G. Impacts of WWEs on biogeochemical variables

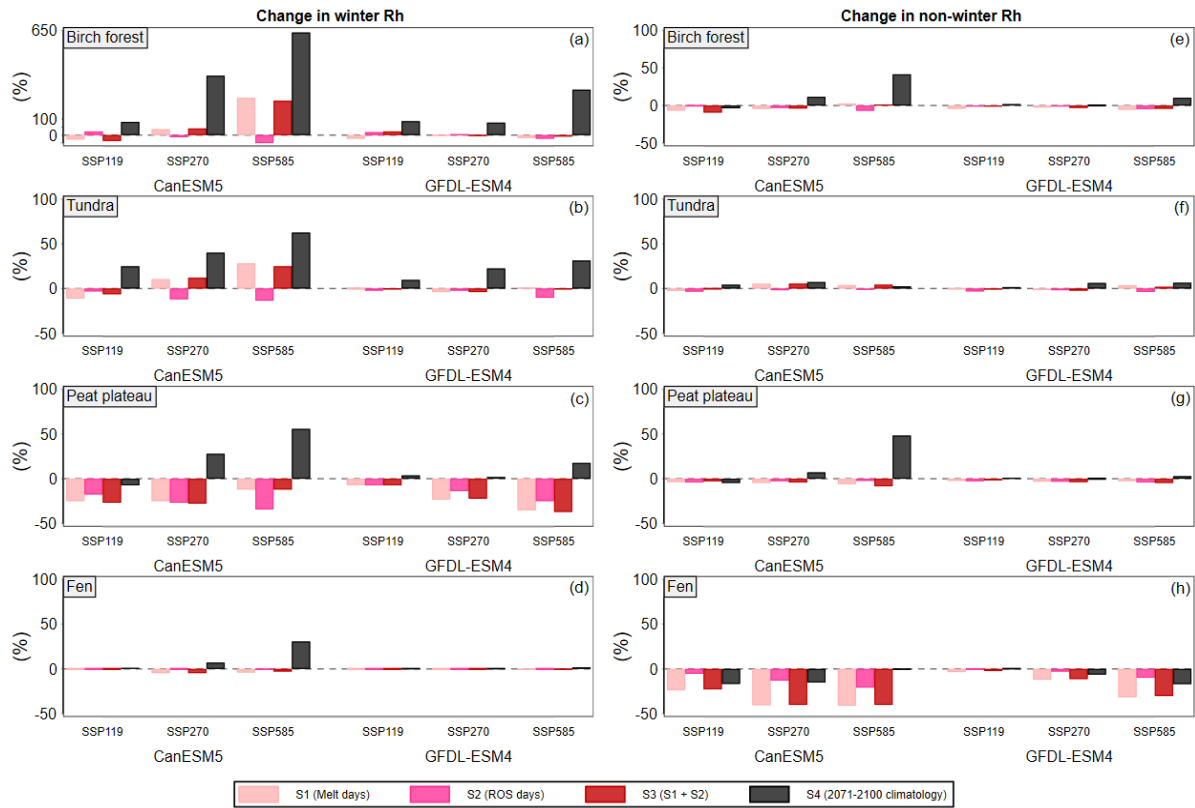


Figure G1. Differences between the model output of the MANIPULATION runs (S1, light pink; S2, pink; S3, red; S4, dark grey) and the HISTORICAL runs (S0), for the variables winter Rh (%) and non-winter Rh (%), at each of the simulated sites. Differences calculated by subtracting each of the MANIPULATION (S1-S4) from the HISTORICAL (S0) simulation outputs.

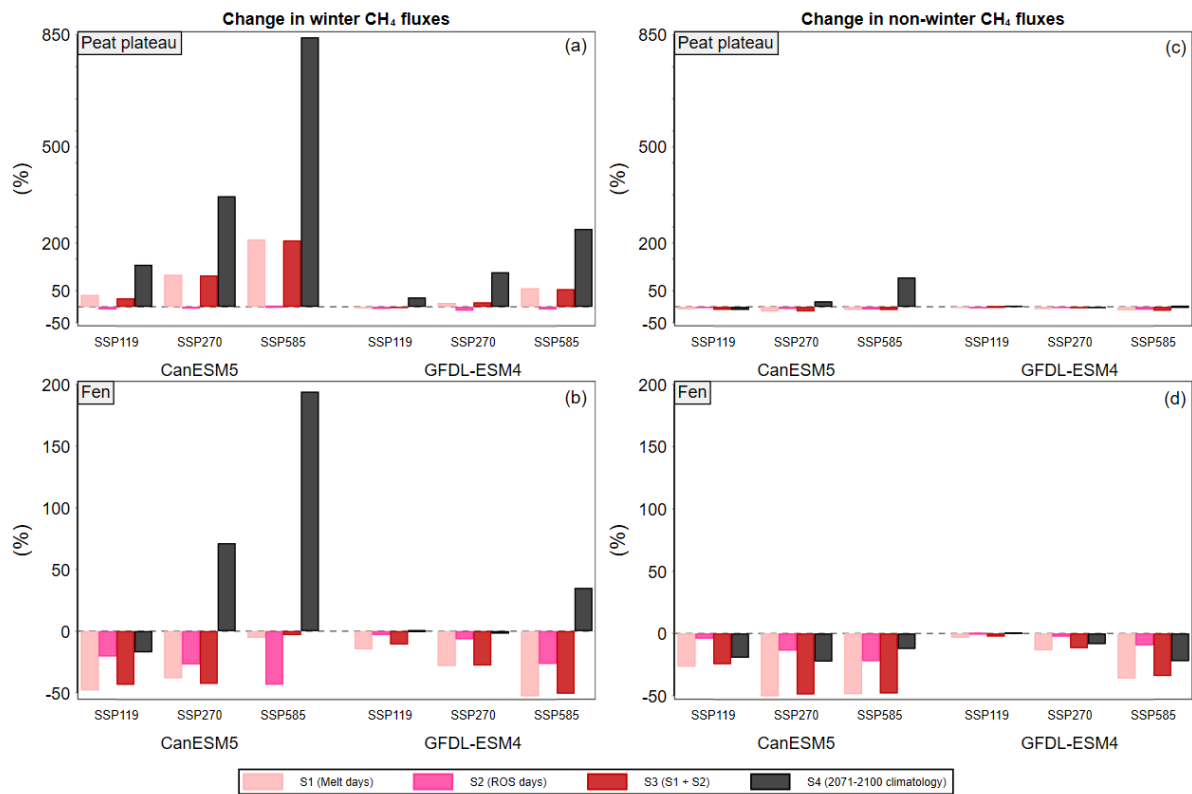


Figure G2. Differences between the model output of the MANIPULATION runs (S1, light pink; S2, pink; S3, red; S4, dark grey) and the HISTORICAL runs (S0), for the variables winter CH₄ and non-winter CH₄ at the peat plateau (a,c) and fen (b,d) sites. Differences calculated by subtracting each of the MANIPULATION (S1-S4) from the HISTORICAL (S0) simulation outputs.

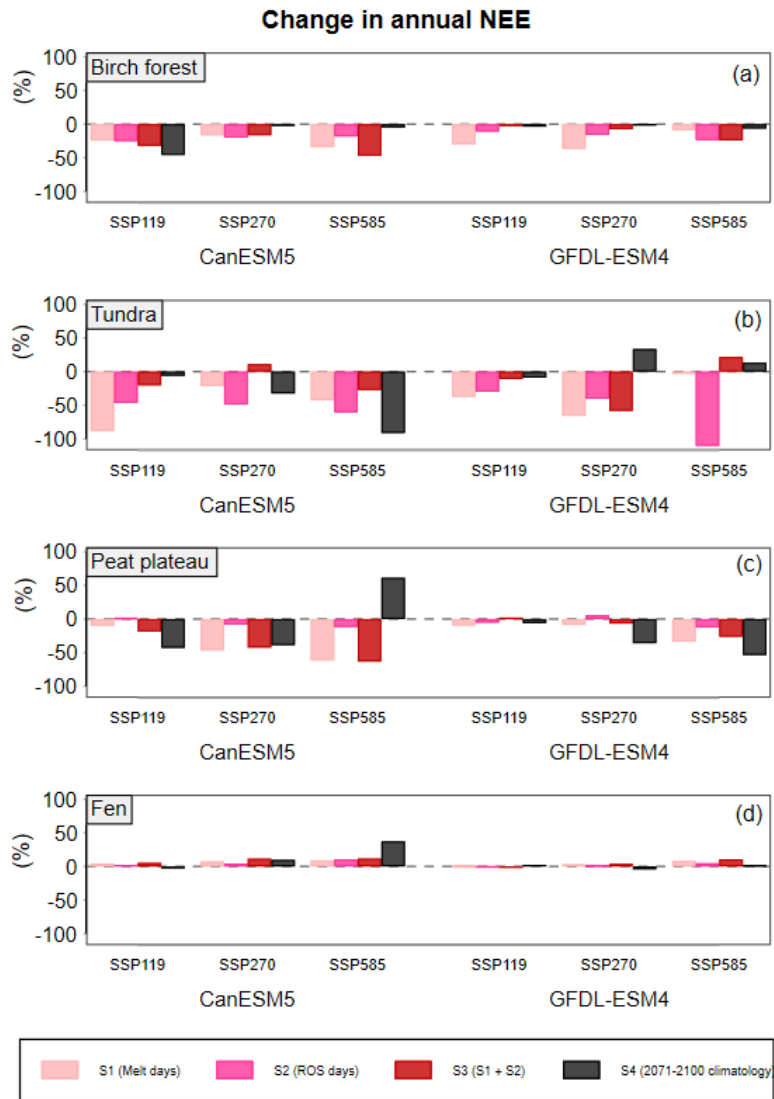


Figure G3. Differences between the model output of the MANIPULATION runs (S1, light pink; S2, pink; S3, red; S4, dark grey) and the HISTORICAL runs (S0), for the variable annual NEE, at the birch forest (a); tundra (b), peat plateau (c), and fen (d) sites. Differences are calculated by subtracting each of the MANIPULATION (S1-S4) from the HISTORICAL (S0) simulation outputs. The positive increases of NEE represent the increases in ecosystem uptake of CO₂, and vice versa.